

A Perturbation/Correlation Approach to Force-Guided Robot Control

by

Sooyong Lee

B.S.M.E. Seoul National University, Seoul, KOREA, 1989

M.S.M.E. Seoul National University, Seoul, KOREA, 1991

**Submitted to the Department of Mechanical Engineering
in Partial Fulfillment of the Requirements for the Degree of**

DOCTOR OF PHILOSOPHY

at the

MASSACHUSETTS INSTITUTE OF TECHNOLOGY

JUNE 1996

Copyright. Massachusetts Institute of Technology 1996
All rights reserved

Signature of Author _____
Department of Mechanical Engineering
May 14, 1996

Certified by _____
Haruhiko Asada
Professor of Mechanical Engineering
Thesis Supervisor

Accepted by _____
Ain A. Sonin
Chairman, Department Committee on Graduate Students

MASSACHUSETTS INSTITUTE
OF TECHNOLOGY

JUN 27 1996

ENG.

LIBRARIES

A Perturbation/Correlation Approach to Force-Guided Robot Control

Sooyong Lee

Abstract

Force guided robot control is a control scheme based on the interpretation of measured force acting on the robot end effector. A functional map relating the correction of motion to force measurements is generated based on the geometry of the workpiece and its kinematic behavior in interacting with the environment. In the traditional force-guided control schemes, the contact force measured by a force sensor is directly fed back to a feedback controller to generate a motion correction signal. However, the force information obtained at one point does not always contain sufficient information to determine the direction of motion. The forces measured are often erratic and noisy due to the friction at the contacting surfaces and the existence of irregular burrs. This often leads to a misjudgment of contact configurations and erratic control actions. Also, the erratic force feedback may lead to excessive contact forces and large friction, which impede smooth motion and incur jamming and damage to the objects. Therefore, it is important to maintain the contact force at an appropriate level. The issue central to force guided robot control is how to obtain reliable, consistent and copious force signals and extract useful information in order to successfully guide the robot while keeping the contact force at a desired level.

In this thesis, instead of simply measuring contact forces, we take positive actions by giving perturbation to the end effector and observing the reaction forces to the perturbation in order to obtain much richer and more reliable information. By taking the correlation between the input perturbation and the resultant reaction forces, we can determine the gradient of the force profile and guide the part correctly. By applying a type of direct adaptive control, the contact force is maintained at the lowest level. This algorithm is applied to a pipe insertion task, in which the insertion force is minimized during the insertion. Based on the process model and stability analysis using the Popov stability criterion, conditions for stable, successful insertion despite nonlinearities and uncertainties in the environment are obtained. The theoretical results are verified using the experimental data. To generate high frequency perturbation, a vibratory end effector using piezoelectric actuators is designed and built. Also, this perturbation/correlation method is applied to a box palletizing task, in which a rectangular box is to be located in one corner of the wall while maintaining constant contact with the wall. Through both simulations and experiments, the feasibility and usefulness of these methods are demonstrated.

Thesis Committee :

Haruhiko Asada
Kamal Youcef-Toumi
Frank Feng

Professor, Mechanical Engineering
Professor, Mechanical Engineering
Professor, Mechanical Engineering

Contents

1 Introduction

1.1 Issues and Previous Work	8
1.2 Objectives and Outline of the Thesis	11

2 Control Architecture

2.1 Introduction	14
2.2 Perturbation/Correlation	14
2.3 Application to the Force Guided Robot	19

3 Case Study : Pipe Insertion Task

3.1 Introduction	27
3.2 Pipe Insertion Task	27
3.3 Modeling of the Process	31
3.4 Selection of Parameters	35
3.5 Simulation	37
3.6 Extension to Three Dimension	38

4. Stability Analysis

4.1 Introduction	42
4.2 Linear System	42
4.3 Nonlinear and Unknown System	44
4.4 Simulation	50

5 Experiment and Implementation

5.1 Introduction	54
5.2 Vibratory End Effector using Piezo Electric Actuator	54
5.3 Experimental Setup	57
5.4 Experimental Data	59
5.5 Comparison with Other Force-Guided Controller	61
5.6 Friction Reduction Due to Perturbation	63

6. Application to the Connector Assembly Task

6.1 Introduction	67
6.2 Connector Assembly	67
6.3 Modeling	69
6.4 Perturbation/Correlation based Control	73
6.5 Simulation.	76
6.6 Comparison with Pipe Insertion Task	78

7. Conclusion

7.1 Contributions	80
7.2 Further Work	81

Reference

List of Figures

Figure 1-1. Force guided control	8
Figure 1-2. Symmetric position-force relationship	10
Figure 2-1. Performance index F and input p	15
Figure 2-2. Perturbation Method	16
Figure 2-3. Linear Regression	16
Figure 2-4. Time-Varying System	18
Figure 2-5. Robot with Environment	20
Figure 2-6. Robot Dynamics	20
Figure 2-7. Robot with Position Controller	20
Figure 2-8. Simplified Representation	21
Figure 2-9. Performance Index	21
Figure 2-10. Perturbation/Correlation	21
Figure 2-11. Gradient of the Performance Index	22
Figure 2-12. Robot System with Perturbation/Correlation	24
Figure 2-13. System with Linear and Nonlinear Block	25
Figure 2-14. Implementation of the Controller	26
Figure 3-1. Pipe insertion task	28
Figure 3-2. Obstructing force F_z v.s. displacement x	29
Figure 3-3. Robot with Perturbation/Correlation	30
Figure 3-4. Insertion force varies depending on x , z and \dot{z}	31
Figure 3-5. Experimental Setup	32
Figure 3-6. F_z as a function of x and z	33
Figure 3-7. F_z as a function of z and \dot{z}	33

Figure 3-8. System modeling	34
Figure 3-9. Block diagram representation	34
Figure 3-10. Simulation Result	38
Figure 3-11. End Effector Trajectory	41
Figure 3-12. Performance Index Time History	41
Figure 4-1. Block diagram representation	43
Figure 4-2. System with nonlinearity	45
Figure 4-3. Nonlinearity	46
Figure 4-4. Displacement vs. Force	46
Figure 4-5. Plot of transfer function	49
Figure 4-6. Simulation Results for Linear Case	52
Figure 4-7. Nonlinear Force Function	52
Figure 4-8. Simulation Results for Nonlinear Case	53
Figure 5-1. Vibratory Endeffector	55
Figure 5-2. Isolated view of the End Effector Head	55
Figure 5-3. Movement of the End Effector	56
Figure 5-4. Vibratory End Effector with Piezo Electric Actuators.	56
Figure 5-5. Vibratory End Effector Mounted on a Force Sensor	57
Figure 5-6. Experimental Setup	58
Figure 5-7. Pipe Insertion by Robot	58
Figure 5-8. Experimental Data	59
Figure 5-9. Verification of the Eq (5-1)	60
Figure 5-10. Compliance Center	61
Figure 5-11. X-displacement and Force Response of the Robot Dither Case	62
Figure 5-12. Comparison with Conventional Controller	63
Figure 5-13. Experiment Setup	64
Figure 5-14. Force Profile with Perturbation	65

Figure 5-15. Resistant Force Comparison	66
Figure 6-1. Connector Assembly	68
Figure 6-2. Reaction Forces	70
Figure 6-3. Coordinates	71
Figure 6-4. Contact Points of the Box	72
Figure 6-5. Performance Index, X, Y, and Theta	77
Figure 6-6. Movement of the Connector	78

1.1 Issues and Previous Work

Force guided robot control is a control scheme based on a stored map from forces to a correction of motion. As shown in Figure 1-1, the motion command is generated through the interpretation of the measured force at the block termed, the "force-to-motion map". Based on the geometry of the workpiece and its kinematic behavior in interacting with the environment, the functional map relating the correction of motion to force measurements is generated. In the past, various methods for designing this map have been developed. [Hanafusa, Asada, 1977], [Whitney, 1977], [Peshikin, 1992]

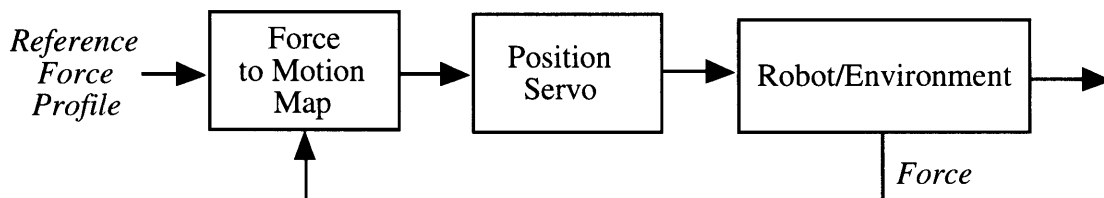


Figure 1-1. Force guided control

The force feedback law may be a simple compliance control law, an admittance control law, or a complex nonlinear control law described by a functional relationship between motion correction signals and the measured force, position, and velocity signals. For more complex tasks, the block of force feedback law may include a logical branch controller and a process monitor, which detects contact changes and determines contact configurations during the operation [Whitney, 1987]. Based on the estimated contact configuration, the correction of robot motion is generated for the robot control system [McCarragher, Asada,

1993]. In any case, the feedback law in the traditional force-guided assembly is represented by a map from measured forces and state variables to a motion correction command. It should be noted that the controller simply receives the force signals generated in the assembly process, which are often erratic and noisy.

To improve the reliability and assure assembly operations, in-process monitoring and closed-loop process control are powerful tools. For monitoring an assembly process, the force and moment acting between mating parts are the major sources of information directly related to the assembly process state. Unlike visual information, the force information provides real-time, in-process information during parts mating operations. Therefore, the force information is indispensable for closed-loop assembly process control as well as for in-process monitoring. To make robotic assembly reliable and robust in the face of a high degree of uncertainties, the closed loop control based on force information and in-process monitoring is critically important. The question is how to obtain useful force information despite inherent difficulties.

Although force information is useful and even indispensable in performing a task that involves mechanical contacts and interactions with the environment, the control based on the simple force-to-motion map, sometimes incurs unwanted behavior. One of the problems often encountered in force guided robot control is "undecidable" situations [McCarragher and Asada, 1994]. As shown in Figure 1-2, let us suppose that the goal is to find the position where the reaction force is minimum and the robot should be directed towards decreasing force. Since the force profile is symmetry, the robot cannot decide which way to proceed to reach the goal. The force information obtained at one point does not contain sufficient information to determine the direction of motion. Additional information such as the gradient of the force profile is necessary for determining the appropriate direction.

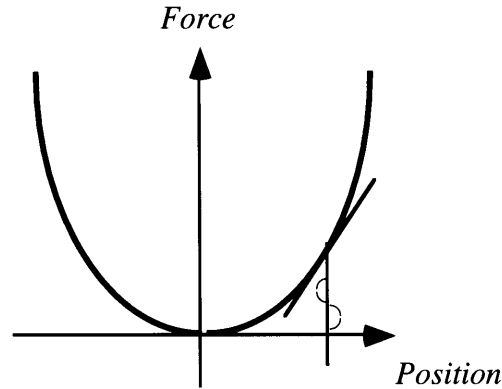


Figure 1-2. Symmetric position-force relationship

The above example illustrates the limit of simple force-to-motion control strategies. Mapping a force measured at one point does not provide complete information to generate a control command. The force-to-motion map must be augmented by combining additional information. In the traditional force-guided assembly scheme, the contact force measured by a force sensor is directly fed into the feedback controller to generate a motion correction signal. The generated force becomes erratic and noisy depending on the smoothness of the contacting surfaces and the existence of irregular burrs so that it may lead to a misjudgment of contact configuration or make control actions erratic. The situation is even worse, when a hand-held object gets stuck or jams at contact points due to irregular burrs. The measured force becomes totally erratic, and so does the control action. Although an object is in contact with a flat surface of the environment, the direction of the contact force varies widely depending on the local roughness of the contacting surfaces. As a matter of fact, a number of parts manually assembled in industry do not have as smooth a surface as the toy blocks we use for research in laboratory environments. The issue central to force guided assembly is how to obtain reliable, consistent and copious force signals and extract useful information from the force signals.

Despite enormous research efforts in the past decades, the assembly techniques developed in the field of robotics have seldom been applied to real manufacturing

processes. Sophisticated techniques such as admittance control [Whitney, 1977], stiffness control [Salisbury, 1980], back projection [Lozano-Perez, Mason and Taylor, 1984] [Erdmann, 1986] and contact recognition [Asada and Hirai, 1989] [Desai and Volz, 1989] [Xiao, 1993] have been developed and tested successfully, but only in laboratory environments. In manufacturing industries, most assembly tasks are performed either manually or by simple machines. Products are designed so that their assembly can be performed simply by standard machines. This so-called *design for assembly* has been the major thrust in today's manufacturing technology. Simplification and standardization must be pursued further, but it should be noted that complex, non-standard parts that cannot be assembled by standard techniques are almost always involved in most products. Such parts, although few in number, are currently very costly as they are assembled manually. Difficult assembly tasks include: i) odd-shaped electronic parts such as connectors, heat sinks, and shields of RF circuits, ii) plastic covers and structures of consumer electronics and appliances, iii) sheet metal and composite parts of automobiles and aircraft, to name a few. These parts are difficult to deal with, since they are highly complex, inaccurate and sometimes deformable, having large tolerance errors. For example, sheet metal parts produced by shearing and stamping are complex and deformable and, more importantly, they have large, sharp burrs that often make assembly operations difficult. When burrs exist, friction becomes highly unpredictable and erratic, preventing smooth mating operations. The assembly operations required for these parts are complicated, yet the task must be performed reliably to meet high quality requirements.

1.2 Objectives and Outline of the Thesis

In this thesis, a novel technique for overcoming the difficulties in the force-guided assembly for real manufacturing applications will be presented. Instead of simply receiving

force information from the assembly process, we give perturbation to the robot end effector and measure the reaction forces to the perturbation. By taking the correlation in between, reliable information for guiding the endeffector will be extracted and used for control. The *dither*, a small amplitude perturbation has been used in many practical ways, but the proposed perturbation/correlation method is different from the previous ones in that the dither is used for the purpose of estimating the gradient of a performance index as well as for friction suppression and that a force feedback loop is formed around the assembly process. Our goal is to guide an assembly part based on force information. Perturbation commands are used as a means to build an effective force feedback loop rather than merely suppressing friction in open loop control.

The technique using perturbation and correlation has been developed, and the undecidable problem shown above was resolved . The end effector is perturbed with a known frequency, in turn the reaction force in response to the perturbation is measured, and its correlation with the perturbation input is computed. The resultant correlation provides the gradient of the force profile, which allows the robot to decide which way to proceed to reach the goal. To implement this method, various parameters including the perturbation frequency and feedback gains must be tuned with care so that the overall stability of the system may be maintained.

The basic concept of perturbation/correlation based control is described in chapter 2 with application to a force guided robot. In chapter 3, we applied this algorithm to a pipe insertion task for a case study. The robot with the environment is modeled with experimental data. A guideline to select several parameters involved in this controller is shown based on the analysis and verified with simulation. In the chapter 4, based on the model, stability analysis is conducted including the unknown nonlinear environment. A vibratory end effector is designed and implemented and with this end effector, the experiment is discussed in chapter 5. Other than the pipe insertion case study, this

perturbation/correlation based control is applied to the connector assembly task in chapter 6 followed by the conclusion.

2.1 Introduction

For a force-guided robot control, the perturbation/correlation based controller is introduced. For most of the assembly tasks by robot, it is required to control the displacement and force. Especially, when there exists uncertainties involved in the assembly task, preprogrammed displacement and force trajectories don't work well. We need to cope with these uncertainties to successfully accomplish the task. Still, the force and displacement are very important information to guide the robot. Our approach is, first set up a performance index which clearly represents the task, and then make a controller to minimize this performance index based on perturbation/correlation. This performance index as well as the control variables we perturb and update should be chosen very carefully. In the following chapters, the basic idea of the perturbation/correlation algorithm is described, and then applied to a force-guided robot system.

2.2 Perturbation/Correlation

The perturbation/correlation method is a direct control method which involves perturbation, correlation and adjustment. For example, consider a plant with appropriate inputs, having unknown environment, and a means of continuously measuring a performance index. The inputs can be changed to affect this performance index. the question is how to adjust this input to get the optimum performance index. The most direct

and simplest procedures would be to adjust the input and see the effect on the performance index. However, in a practical problem, the number of parameters to be adjusted, the presence of output noise, the parameters of the plant may vary with time and nonlinearities may be present in a plant. The feasibility of this method would depend on the stability of the overall system as the plant parameters varied with time. The role of the perturbation is giving variations to the input. The correlation is to estimate the change of the performance index with respect to the change of the input, in other words, the gradient of the performance index. Based on this estimate of the gradient we can adjust the input so that we can minimize the performance index. From now on, we will prove the correlation corresponds to the gradient.

Consider a performance index, F , with input x as in Figure 2-1. Even though we don't know the exact mathematical representation of F , by locally perturbing the input x , we need to estimate $\frac{\partial F}{\partial x}$ around a local region.

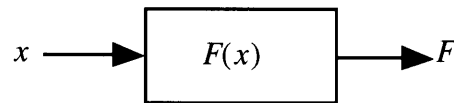


Figure 2-1. Performance index F and input x

Assuming that we can choose the value of x and observe the corresponding value of F at every instant, the objective is to determine a procedure for adjusting x so that it converges to the optimal value, $x_{optimal}$ which give the minimum value of F .

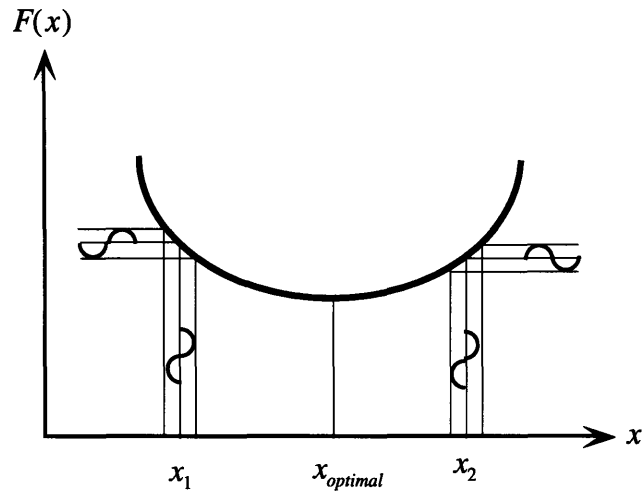


Figure 2-2. Perturbation Method

Let the parameter x be varied sinusoidally around a nominal point, then by observing the variation of the output, and phase difference between the input x and the output $F(x)$, we obtain the direction to adjust the input in order to minimize the output. In [Lee and Asada, 1994], the mathematical relation between the correlation value and the gradient of a function is derived. For a static mapping between the input x and output F as shown in Figure 2-3,

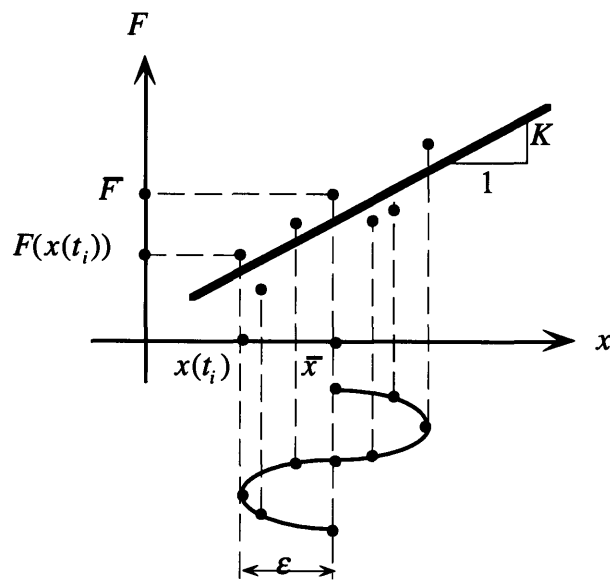


Figure 2-3. Linear Regression

let x be an input command to one of the robot control axes, which is varied sinusoidally around its nominal value, x_o so that

$$x(t) = x_o + \varepsilon \delta_x(t) \quad (2-1)$$

$$\delta_x(t) = \sin(\omega_p t) \quad (2-2)$$

where ε and ω_p are, respectively, the amplitude and frequency of the sinusoidal perturbation. Let $F(x)$ be the performance index corresponding to the input. The correlation between x and $F(x)$ is given by

$$R_x = \int_t^{t+\frac{2\pi}{\omega_p}} \delta_x(\tau) F(x(\tau)) d\tau \quad (2-3)$$

where the integral interval is over one complete period of the perturbation. When the force is sampled at time $t_i = \frac{\pi i}{n\omega_p}$, $i = 1, \dots, 2n$, eq.(2-3) reduces to

$$\hat{R}_x = \sum_{i=1}^{2n} F(t_i) \varepsilon \sin\left(\frac{\pi}{n} i\right) \quad (2-4)$$

From the linear regression, the slope at the point \bar{x} , is defined as

$$K = \frac{\sum_{i=1}^{2n} [x(t_i) - \bar{x}] [F(t_i) - \bar{F}]}{\sum_{i=1}^{2n} [x(t_i) - \bar{x}]^2} \quad (2-5)$$

where,

$$\bar{x} = \frac{1}{2n} \sum_1^{2n} x(t_i) = \bar{x}_o \quad (2-6)$$

$$\bar{F} = \frac{1}{2n} \sum_1^{2n} F(t_i) \quad (2-7)$$

Substituting eq.(2-1) into eq.(2-5) yields

$$K = \frac{\sum_{i=1}^{2n} \varepsilon \sin\left(\frac{\pi}{n} i\right) [F(t_i) - \bar{F}]}{\sum_{i=1}^{2n} \varepsilon^2 \sin^2\left(\frac{\pi}{n} i\right)} = \frac{\sum_{i=1}^{2n} F(t_i) \sin\left(\frac{\pi}{n} i\right)}{n\varepsilon} \quad (2-8)$$

Comparing eq.(2-8) with eq.(2-4),

$$\hat{R}_p = n\varepsilon^2 K \quad (2-9)$$

Namely, the correlation given by eq.(2-4) represents the gradient of the function at the nominal point multiplied by known constants. For the sake of simplicity, the above formulation of correlation is only for one dimensional perturbation. This can be extended to multi-input, multi-output correlations by using standard techniques [Eveleigh,1967]. The above example is based on a static mapping between position and force relationship. We also need to check for time varying system. For a simple system containing a single parameter θ shown in Figure 2-4, the output of the plant is the instantaneous performance index $F(\theta, t)$. The objective is to determine the optimal value θ_{opt} of θ so that the performance index is minimized. The problem of optimization of a time varying system has been reduced to the minimization of the function $\bar{F}(\theta)$ with respect to the parameter θ .

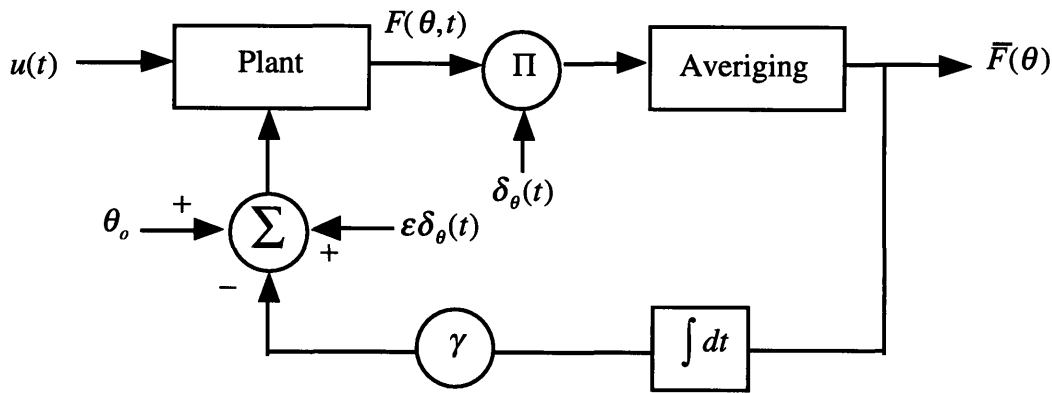


Figure 2-4. Time-Varying System

Assuming that $\theta(t)$ is perturbed around a nominal value θ_o as eq. (2-10),

$$\theta(t) = \theta_o + \varepsilon \delta_\theta(t) \quad (2-10)$$

the change in the performance index may be approximated by

$$\bar{F}[t; \theta_o + \varepsilon \delta_\theta(t)] \approx \bar{F}[t; \theta_o] + \varepsilon \delta_\theta(t) \nabla \bar{F} \Big|_{\theta=\theta_o} \quad (2-11)$$

if \bar{F} is a smooth function of the parameter θ . Correlating $\delta_\theta(t)$ and $\bar{F}[t; \theta_o + \varepsilon \delta_\theta(t)]$, we obtain

$$\overline{\delta_\theta(t)\bar{F}[t;\theta(t)]} \approx \overline{\delta_\theta(t)\bar{F}[t;\theta_o]} + \overline{\varepsilon\delta_\theta^2(t)\nabla_\theta\bar{F}|_{\theta=\theta_o}} \quad (2-12)$$

Assuming that $\delta_\theta(t)$ is independent of the input $u(t)$ and has an average value zero, the first term can be neglected. The second term in eq. (2-12) yields a quantity which is approximately proportional to the gradient of \bar{F} with respect to θ at the operating point θ_o . This quantity is used for updating the parameter θ . A simple gradient descent method allows this system to reach the optimal point. The parameters of interest are the amplitude and frequency of the perturbation and the gain in the feedback loop. Selection of these parameters are discussed in detail in chapter 3 with pipe insertion task, but briefly,

- i) too small a value of the amplitude makes the determination of the gradient difficult while too large a value may overlook the optimum value
- ii) a very high frequency of perturbation may have negligible effect on the output while a low value of it requires a long averaging time.
- iii) a large step size of the which gain may result in hunting or even instability while a small value of it would result in very slow convergence.

2.3 Application to the Force Guided Robot

Consider a robot system which has the internal position controller. The end effector is interacting with an environment doing a task, such as peg-in hole, inserting a pipe or palletizing a box. As the robot moves, in other words, as the displacement of the end effector changes, the force response from the environment would be changed, too. If we could set up a performance index, which clearly represents the task, then by minimizing the performance index, we can successfully finish the task. The question is how we can minimize the performance index. The information we could get is the reaction force, and

what we can change is the displacement of the robot. Therefore, the main idea is, by correctly updating the displacement, we could minimize the performance index, and thereby, accomplish the task. The gradient of the performance index with respect to the displacement would be used to adjust the displacement of the robot.

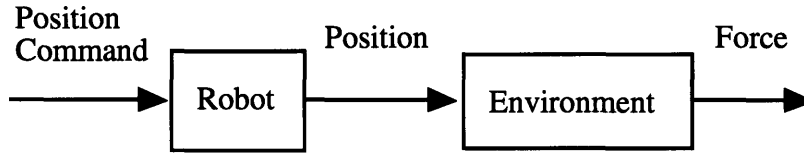


Figure 2-5. Robot with Environment

To formulate this perturbation/correlation based controller applied to the force-guided robot system, we start from the basic robot system model. A linear system model for a robot can be represented in state space form as in eq. (2-13)

$$\dot{X} = AX + Bu \tag{2-13}$$

$$y = CX \tag{2-14}$$

where, X_{nx1} , A_{nxn} , B_{nx1} , C_{1xn}

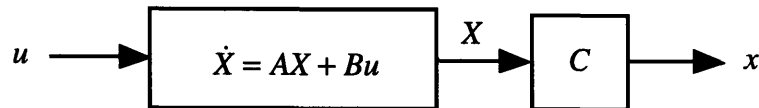


Figure 2-6. Robot Dynamics

For simplicity, a proportional controller was used for the system output, x to follow the desired output, x_d

$$u = k(x_d - x) \tag{2-15}$$

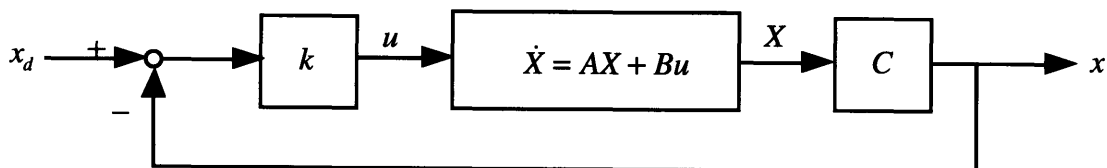


Figure 2-7. Robot with Position Controller

The original system equation with proportional controller can be represented as in Figure 2-8.

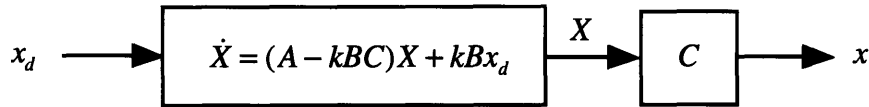


Figure 2-8. Simplified Representation

We have a performance index $\Phi(x)$, which is a function of x .

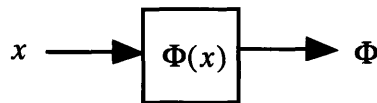


Figure 2-9. Performance Index

and we want to minimize performance index $\Phi(x)$, by changing x . The correlation/perturbation part gives the gradient of $\Phi(x)$ with respect to x , that is, $\frac{\partial \Phi(x)}{\partial x}$.

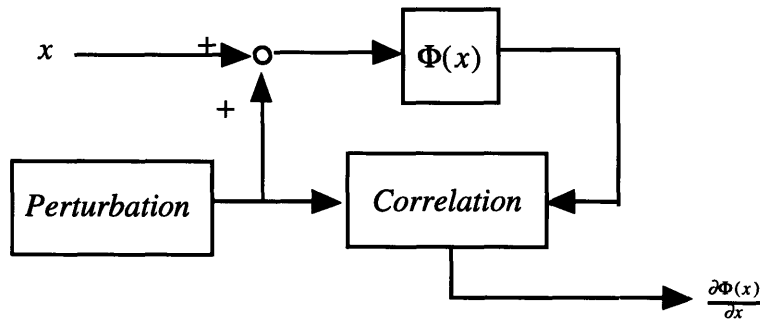


Figure 2-10. Perturbation/Correlation

For this perturbation/correlation part to be represented as a block diagram of which the input is x , and output is $\frac{\partial \Phi(x)}{\partial x}$ shown in Figure 2-11, the following condition should be satisfied.

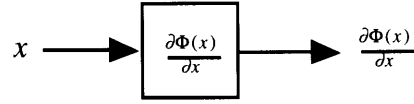


Figure 2-11. Gradient of the Performance Index

A performance index Φ is a function of the input x , and several other variables, z_1, \dots, z_n .

$$\Phi = \Phi(x, z_1, \dots, z_m, z_{m+1}, \dots, z_n) \quad (2-16)$$

To get $\frac{\partial \Phi}{\partial x}$, we perturb the input x as in eq. (2-17)

$$x(t) = x_o + \delta_x(t) \quad (2-17)$$

Let's assume that some of the other variables also have perturbations. For $i = 1 \dots m$

$$z_i(t) = z_{o,i} + \delta_{z,i}(t) \quad (2-18)$$

and for $i = (m+1) \dots n$

$$z_i(t) = z_{o,i} \quad (2-19)$$

Assuming that Φ is differentiable with respect to y and z_1, \dots, z_n , Φ is expanded as :

$$\begin{aligned} & \Phi[x(\tau + \Delta t), z_1(\tau + \Delta t), \dots, z_n(\tau + \Delta t)] \\ &= \Phi[x(\tau), z_1(\tau), \dots, z_n(\tau)] + \delta_x(t) \frac{\partial \Phi}{\partial x} \Big|_{\tau} + \delta_{z,1}(t) \frac{\partial \Phi}{\partial z_1} \Big|_{\tau} + \dots + \delta_{z,n}(t) \frac{\partial \Phi}{\partial z_n} \Big|_{\tau} + \vartheta(2) \end{aligned} \quad (2-20)$$

ignoring the higher order term, $\vartheta(2)$, and because $\delta_{z,i}(t)$ is zero for $i = (m+1) \dots n$, eq.

(2-20) becomes

$$\Phi[x(\tau), z_1(\tau), \dots, z_n(\tau)] + \delta_x(t) \frac{\partial \Phi}{\partial x} \Big|_{\tau} + \delta_{z,1}(t) \frac{\partial \Phi}{\partial z_1} \Big|_{\tau} + \dots + \delta_{z,m}(t) \frac{\partial \Phi}{\partial z_m} \Big|_{\tau} \quad (2-21)$$

Correlating Φ and δ_x , and taking average for one period of perturbation : $[0, \frac{2\pi}{\omega}]$, we obtain

$$\begin{aligned} \overline{\delta_x \Phi} \approx & \int_{\tau-2\pi/\omega}^{\tau} \Phi[x(\tau), z_1(\tau), \dots, z_m(\tau)] \delta_x(t) dt + \\ & \int_{\tau-2\pi/\omega}^{\tau} \delta_x(t)^2 \frac{\partial \Phi}{\partial x} \Big|_{\tau} dt + \int_{\tau-2\pi/\omega}^{\tau} \delta_x(t) \delta_{z_1}(t) \frac{\partial \Phi}{\partial z_1} \Big|_{\tau} dt + \dots + \int_{\tau-2\pi/\omega}^{\tau} \delta_x(t) \delta_{z_m}(t) \frac{\partial \Phi}{\partial z_m} \Big|_{\tau} dt \end{aligned} \quad (2-22)$$

We are perturbing $\delta_x(t)$ sinusoidally as in eq. (2-23)

$$\delta_x(t) = \varepsilon \sin \omega t \quad (2-23)$$

therefore, eq. (2-22) becomes

$$\overline{\delta_x \Phi} = \varepsilon^2 \pi \frac{\partial \Phi}{\partial x} \Big|_{\tau} + \frac{\partial \Phi}{\partial z_1} \Big|_{\tau} \int_{\tau-2\pi/\omega}^{\tau} \delta_x(t) \delta_{z_1}(t) dt + \dots + \frac{\partial \Phi}{\partial z_m} \Big|_{\tau} \int_{\tau-2\pi/\omega}^{\tau} \delta_x(t) \delta_{z_m}(t) dt \quad (2-24)$$

The first term in eq. (2-24) vanishes and the second term provides the gradient $\frac{\partial \Phi}{\partial x}$ multiplied by a known constant $\varepsilon^2 \pi$. The remaining terms should be zero or made negligibly small. If we check eq. (2-25)

$$\int_{\tau-2\pi/\omega}^{\tau} \delta_x(t) \delta_{z_i}(t) dt \quad (2-25)$$

this term becomes zero when $\delta_x(t)$ and $\delta_{z_i}(t)$ are orthogonal, for example,

$$\delta_{z_i}(t) = \varepsilon_i \cos \omega t \quad (2-26)$$

then,

$$\int_{\tau-2\pi/\omega}^{\tau} \delta_x(t) \delta_{z_i}(t) dt = 0 \quad (2-27)$$

In case the variable $\delta_{z,i}$ changes linearly with respect to time as in eq. (2-28)

$$\delta_{z,i}(t) = \varepsilon_i t \quad (2-28)$$

then, eq. (2-25) becomes

$$\int_{\tau=2\pi/\omega}^{\tau} \delta_x(t) \delta_{z,i}(t) dt = -\frac{2\pi\varepsilon\varepsilon_i}{\omega^2} \quad (2-29)$$

Since it is inversely proportional to ω^2 and proportional to ε_i , we can make this term negligibly small by increasing the perturbation frequency ω with small ε_i . Based on this gradient value $\frac{\partial\Phi}{\partial x}$, we update x so that we can decrease performance index as in eq. (2-30).

$$x_d = x_o - \gamma \int_0^t \frac{\partial\Phi(x)}{\partial x} d\tau \quad (2-30)$$

For this perturbation/correlation control, a feedback loop was implemented to update the desired output in order to minimize the performance index $\Phi(x)$.

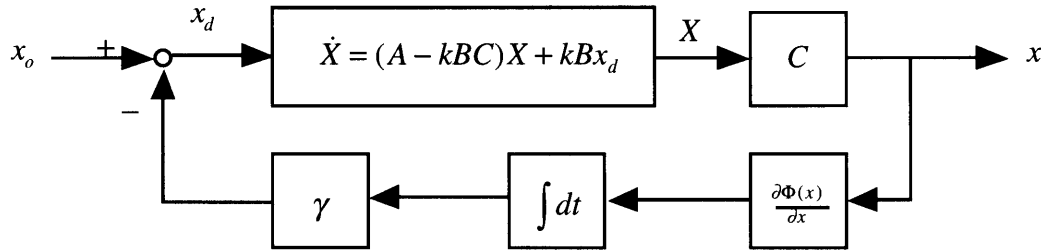


Figure 2-12. Robot System with Perturbation/Correlation

We showed in the previous section that the correlation/perturbation algorithm gives the gradient value of the performance index. By introducing an extra variable, x_a , the augmented system can be represented as in eq. (2-32) and eq. (2-34)

$$x_a = x_d \quad (2-31)$$

$$\dot{x}_a = -\gamma \frac{\partial\Phi(x)}{\partial x} \quad (2-32)$$

$$\begin{Bmatrix} \dot{X} \\ \dot{x}_a \end{Bmatrix} = \begin{bmatrix} A - kBC & kB \\ 0_{1 \times n} & 0 \end{bmatrix} \begin{Bmatrix} X \\ x_a \end{Bmatrix} + \begin{Bmatrix} 0_{n \times 1} \\ -\eta \end{Bmatrix} \frac{\partial \Phi(x)}{\partial x} \quad (2-33)$$

$$x = \begin{bmatrix} C & 0 \end{bmatrix} \begin{Bmatrix} X \\ x_a \end{Bmatrix} \quad (2-34)$$

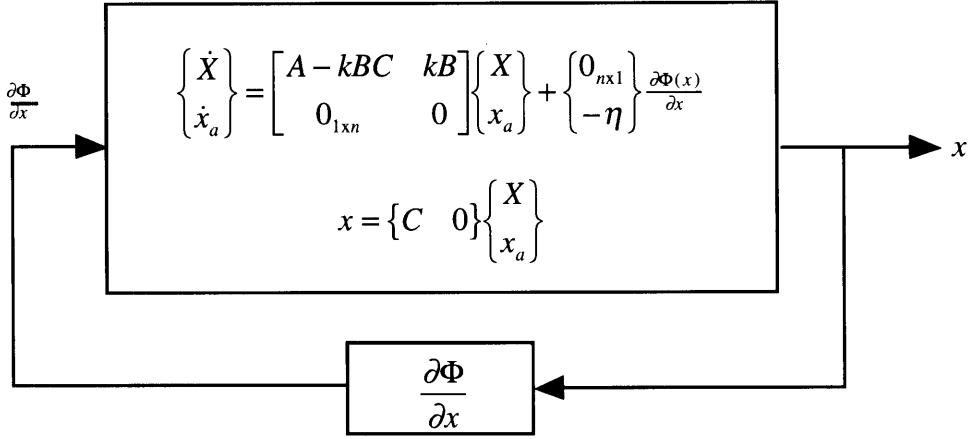


Figure 2-13. System with a Linear and a Nonlinear Block

depending on the performance index $\Phi(y)$, this system of equations can be simplified, and various stability analysis can be conducted. For example, if we introduce a new vector, Z such as,

$$Z = \begin{Bmatrix} X \\ x_a \end{Bmatrix} \quad (2-35)$$

$$\dot{Z} = FZ + G \frac{\partial \Phi(y)}{\partial y} \quad (2-36)$$

$$F = \begin{bmatrix} A - kBC & kB \\ 0_{1 \times n} & 0 \end{bmatrix} \quad (2-37)$$

$$G = \begin{Bmatrix} 0_{n \times 1} \\ -\eta \end{Bmatrix} \quad (2-38)$$

$$x = HZ \quad (2-39)$$

$$H = \begin{bmatrix} C & 0 \end{bmatrix} \quad (2-40)$$

where, $Z_{(n+1) \times 1}$, $F_{(n+1) \times (n+1)}$, $G_{(n+1) \times 1}$, $H_{(n+1) \times 1}$

Based on this final system model, we can apply stability criterion. With the separated linear part, and nonlinear part, this model is useful for applying nonlinear stability theory.

The implementation of the perturbation/correlation based controller for the force-guided robot is represented in Figure 2-14, where γ is the feedback gain. Based on this gradient information, we can implement a controller of which the goal is to minimize a performance index, F . A simple gradient descent method allows the robot to reach the optimal point.

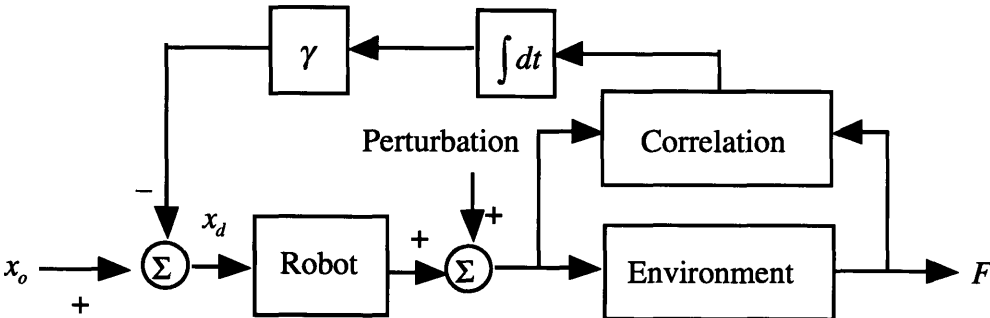


Figure 2-14. Implementation of the Controller

For this trajectory modification loop to work correctly, the correlation signal must not have a significant phase lag : otherwise the correct gradient of the performance index can not be obtained. However, due to the low bandwidth of the robot system, we need another device to generate the high frequency vibration rather than moving the whole robot body. We designed and implemented the vibratory end effector for this purpose and that will be discussed later in detail. Also, several parameters involved in this algorithm should be tuned to guarantee the overall system stability. These are discussed in the following chapter.

Chapter 3

Case Study : Pipe Insertion Task

3.1 Introduction

We formulated the correlation/perturbation based controller for a force-guided robot in the previous chapter. For a case study, we applied this control algorithm for a robot which inserts a pipe into a heat exchanger. As the robot inserts a copper pipe into the hole of the heat exchanger, the pipe interacts with the layers of metal foils. First, we selected the resistant force as a performance index for this task. By adjusting the position of the robot end effector, we can reduce the performance index and successfully insert the pipe. The characteristic of the force response is very nonlinear and simple 'force to position' map is not working very well for this task. We modeled this robot and environment based on the analytic model and experimental data. Also the guideline to select several parameters involved in this algorithm is discussed with simulation result.

3.2 Pipe Insertion Task

The perturbation/correlation based control is applied to a practical assembly task, which is difficult to perform by traditional methods. Figure 3-1 shows the assembly of a heat exchanger for an air conditioning system.

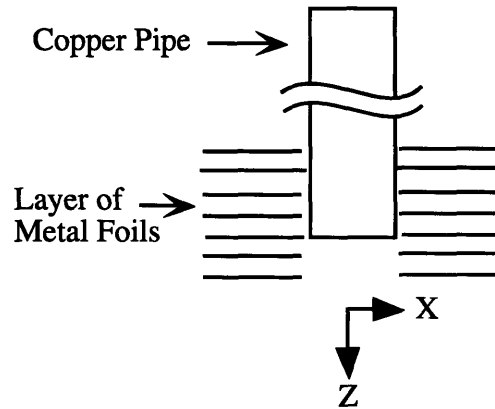


Figure 3-1. Pipe insertion task

The task is to insert a long copper pipe into a stack of thin sheet metals. The holes on the sheet metal have a minimum clearance, in order to maximize the heat transfer efficiency. Unlike the conventional peg insertion problem which deals with machined parts with clear edges and surfaces, the surface of the hole created by the stack of aluminum foils is totally irregular and rugged. Since the aluminum foils are made by stamping, the hole has irregular burrs and poor tolerance error. As a result, the accuracy in fixturing the foils become significantly low, and the wall of the holes created by the stack of the foils is irregular as shown in the figure. In real plant production lines, this kind of pipe insertion task has been performed only by human workers. Skilled workers insert pipes by perturbing the pipes in order to avoid jamming as well as to determine which way to correct the motion. According to them, the skilled workers monitor obstructing forces in response to the applied perturbation, and modify their motion accordingly. Their skill is very similar to our force sensing method described in the previous chapter.

The key information used in the pipe insertion is the reaction force in the pipe's longitudinal direction, that is, the Z axis in Figure 3-1. This obstructing force, F_Z , varies in accordance with the perturbation of the pipe in the transversal direction, that is, the x axis in the figure. The correlation in between is given by

$$R_x(t) = \int_{t-T}^t F_z(\tau) \varepsilon \sin(\omega_p \tau) d\tau \quad (3-1)$$

The obstructing force is created at the contacts of the pipe against the wall of the holes. As the pipe trajectory deviates from the center line of the hole, the obstructing force generally increases, because the pipe's contact pressure against the wall of the hole increases. A smaller obstructing force implies that the pipe's position is closer to the actual centerline, where the pipe can be inserted smoothly. Therefore, we can use the obstructing force as an index representing the deviation of the pipe's trajectory for the purpose of guiding the pipe in the desirable direction. Figure 3-2 shows an approximate plot of F_z against displacement x . The minimum point in the figure shows the plausible centerline position to which the pipe's trajectory is to be corrected during the insertion.

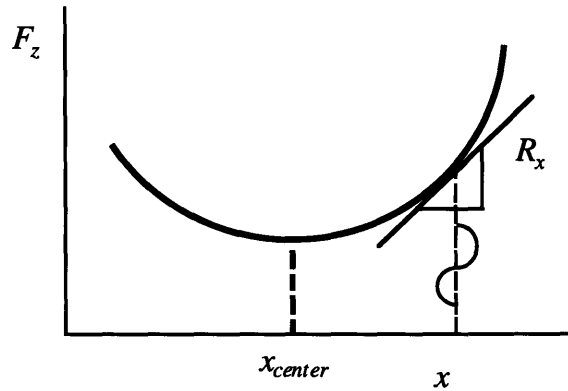


Figure 3-2. Obstructing force F_z v.s. displacement x

In order to guide the pipe towards the minimum point of force F_z , we need to know the gradient of the curve or its equivalent information. Note that the force measured at a single point does not provide sufficient information as to which way the robot should move. This is an undecidable situation. The correlation $R_x(t)$ given by eq.(3-1) resolves this problem since it directly provides the gradient information, as analyzed in the previous section. Therefore, the control law to correct the trajectory of the pipe is simply given by

$$\frac{dx_d}{dt} = -\gamma R_x(t) \quad (3-2)$$

where x_d is the trajectory command to the x axis servo, and γ , the proportional constant. Figure 3-3 shows the block diagram of the x axis control system, in which the nominal trajectory x_o is corrected based on the correlation R_x in accordance with eq.(3-2).

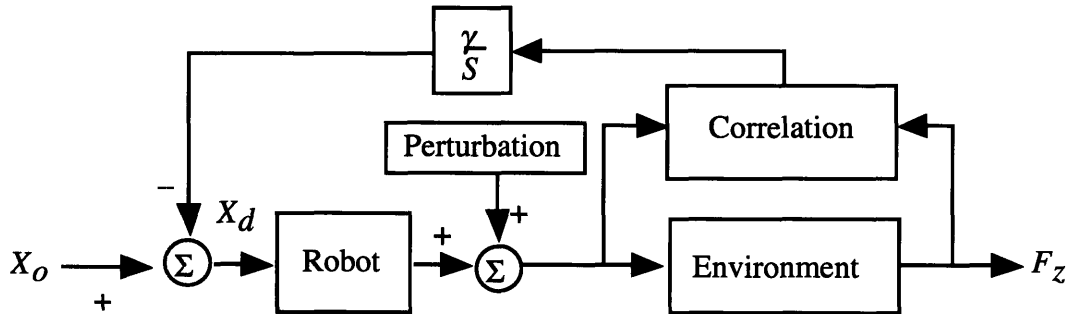


Figure 3-3. Robot with Perturbation/Correlation

This control system can be regarded as a type of direct adaptive control [Narendra and Annaswamy, 1989], since the control system is driven towards the minimum point of performance index F_z , directly by perturbing the control command x_o . It should be noted that the force measured is by no means a clear signal. The actual plot of F_z , against x is an erratic, noisy one, unlike the conceptual plot in Figure 3-2. Nevertheless, the system can behave smoothly because the correlation operation requires integral operations rather than derivatives. To obtain the gradient information, we usually need derivative operations, but this correlation method does not need derivatives but integrals, which are much smoother and computationally more stable. For perturbation, we generate vibration using vibratory end effector, so that we can not only generate high frequency dither, but also the whole robot arm doesn't have to shake the whole arm. Also, we can separate the perturbation part with robot controller, so that it makes easier to apply the stability theorem.

3.3 Modeling of the Process

In this pipe insertion task, the robot end effector is perturbed in the x direction and the x coordinate of its trajectory is corrected while moving in the z direction at a constant speed. The x coordinate is updated based on the insertion force F_z , in such a way that the x coordinate is moved towards the minimum point of F_z . Insertion force F_z is a function not only of the x coordinate but also of the depth of insertion z and the insertion speed \dot{z} . As the depth of insertion increases, more aluminum foils may contact with the pipe and generate a larger resistive force when the pipe is pushed into the hole. Therefore, as z increases, F_z increases in general. Also, the resistive force varies depending on the insertion velocity \dot{z} . Hence, F_z is expressed as

$$F_z = \Phi(x, z, \dot{z}) \quad (3-3)$$

Function Φ is an unknown function, but can be assumed that it has a minimum point with respect to x .

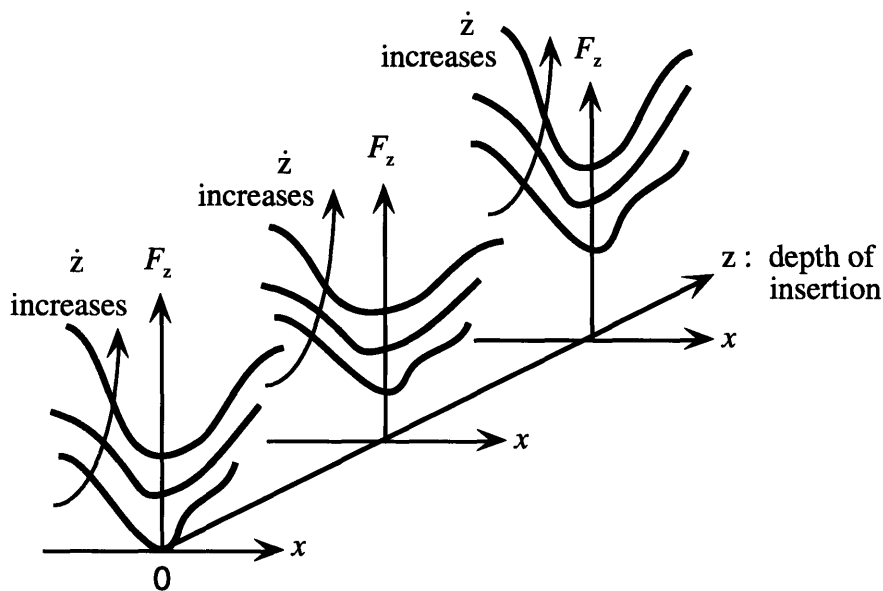


Figure 3-4 Insertion force varies depending on x , z and \dot{z}

As shown in Figure 3-4, although the profile of function Φ varies depending on z and \dot{z} , it is assumed that the function has a minimum with respect to x in each stage of insertion as long as the insertion speed is constant. This assumption is supported by experimental data, as will be discussed later.

We assumed F_z is a function of x and z coordinates and also the velocity \dot{z} . Also, it has a minimum point with respect to x . To verify this assumption, we collected experimental data with many different conditions as in Figure 3-5.

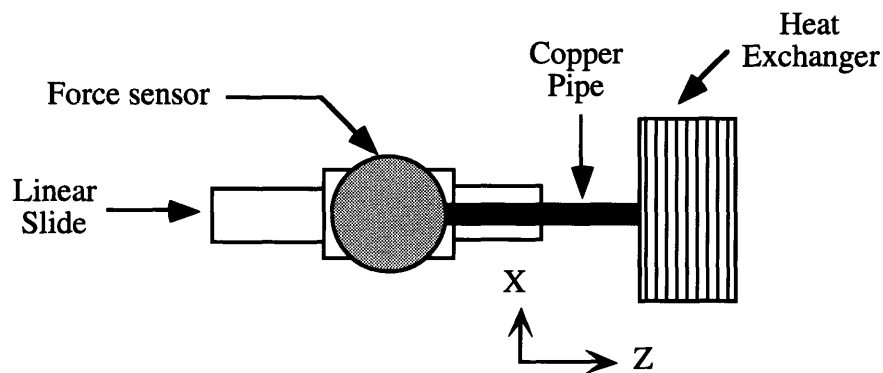


Figure 3-5. Experimental Setup

Note that the displacement in the x -direction is fixed until it reaches the desired depth, and the velocity in the z -direction is kept constant for each run. First of all, the resistant force F_z is measured with slightly different x coordinates so that we could check that it has a minimum point. We plotted the minimum resistant force profile with two nearby ones. This experiment was repeated with several different velocity \dot{z} . One of them is shown in Figure 3-5 and we obtained similar results with different velocities.

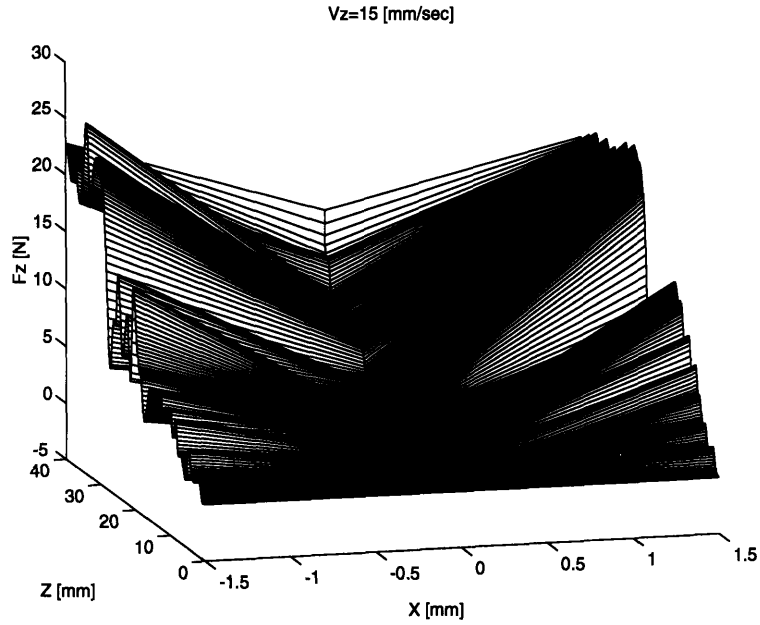


Figure 3-6. F_z as a function of x and z

Figure 3-6 clearly shows that F_z has a minimum point with respect to x . Figure 3-7 shows F_z with different velocity \dot{z} . From this figure, F_z is also a function of \dot{z} , but it doesn't highly depend on \dot{z} . From these result, we verified that the F_z satisfies our assumption.

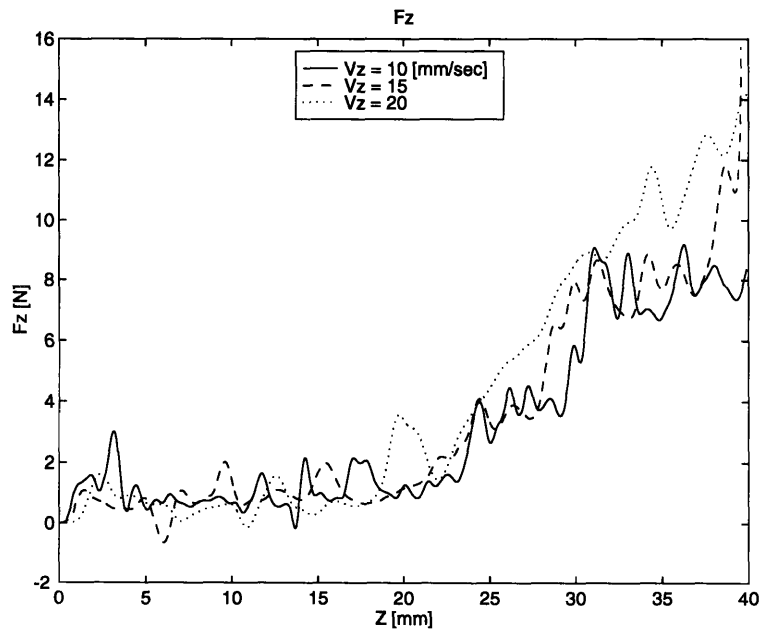


Figure 3-7. F_z as a function of z and \dot{z}

From these result, we verified that the F_z satisfies our assumption.

Based on the experimental verification, we can model the system without including the movement in z -direction as second order system with mass m , damper b and spring K_e due to the environmental stiffness. The displacement of the robot is represented as x_r .

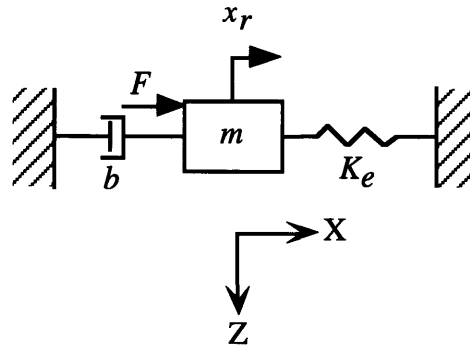


Figure 3-8. System modeling

$$m\ddot{x}_r = -b\dot{x}_r - K_e x_r + F \quad (3-4)$$

Control force is generated using a proportional controller.

$$F = K_p(x_d - x_r) \quad (3-5)$$

The trajectory command, x_d is generated based on the algorithm shown in Figure 3-9. It is represented in eq. (3-6).

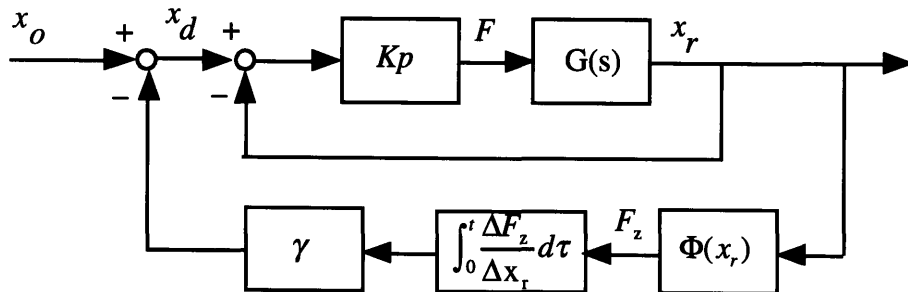


Figure 3-9. Block diagram representation

$$x_d = x_o - \gamma \int_0^t \frac{\Delta F_z}{\Delta x_r} d\tau \quad (3-6)$$

where, γ is a positive update constant and the initial nominal trajectory x_o is usually zero.

To represent this system in a state space form, let

$$x_1 = x_r \quad (3-7)$$

$$x_3 = \int_0^t \frac{\partial F_z}{\partial x_1} d\tau \quad (3-8)$$

Then, the system equation is,

$$\dot{x}_1 = x_2 \quad (3-9)$$

$$\dot{x}_2 = -\frac{K_e + K_p}{m} x_1 - \frac{b}{m} x_2 - \gamma \frac{K_p}{m} x_3 \quad (3-10)$$

$$\dot{x}_3 = \frac{\partial F_z}{\partial x_1} \quad (3-11)$$

3.4 Selection of Parameters

In this perturbation/correlation based control, there are several variables we should select. For perturbation itself, we need to choose the values of amplitude and frequency of the perturbation. For the feedback controller, we need to tune the feedback gain. This gain is related to the stability of the system, and is discussed in the next chapter. The amplitude of the perturbation is constrained by the geometry of the hole and the pipe. Especially, for this heat exchanger, small clearance should be kept for heat conductivity. Therefore, we'd better use small amplitude for perturbation. However, if we use too small amplitude, we can't get meaningful force response but only the noisy signal. For the frequency, we can guess that the higher is better, to get faster update. In this section, we do analysis to see the effects of these variables.

Since the function Φ is unknown, we perturb the end effector in order to obtain the gradient $\frac{\partial F_z}{\partial x}$ as mentioned in the previous section.

$$x(t) = x_o + \delta_x(t) \quad (3-12)$$

$$\delta_x(t) = \varepsilon \sin \omega t \quad (3-13)$$

The insertion speed is kept constant with a high gain position control in the z axis :

$$z(t) = z_o + V_o t \quad (3-14)$$

Consider the insertion force F_z at time $t = \tau + \Delta t$. Assuming that F_z is differentiable with respect to x and z , F_z is expanded as :

$$F_z[x(\tau + \Delta t), z(\tau + \Delta t), V_o] = F_z[x(\tau), z(\tau), V_o] + \delta_x(t) \frac{\partial \bar{F}_z}{\partial x} \Big|_{\substack{x=x(\tau) \\ z=z(\tau)}} + \delta_z(t) \frac{\partial \bar{F}_z}{\partial z} \Big|_{\substack{x=x(\tau) \\ z=z(\tau)}} + \vartheta(2) \quad (3-15)$$

where $\delta_z = V_o \Delta t$ and $\vartheta(2)$ is a higher order small quantity. Correlating F_z and δ_x , and taking average for one period of perturbation : $[0, \frac{2\pi}{\omega}]$, we obtain

$$\overline{\delta_x F_z} \approx \int_{\tau-2\pi/\omega}^{\tau} F_z[x(\tau), z(\tau), V_o] \delta_x(t) dt + \int_{\tau-2\pi/\omega}^{\tau} \delta_x(t)^2 \frac{\partial \bar{F}_z}{\partial x} \Big|_{\substack{x=x(\tau) \\ z=z(\tau)}} dt + \int_{\tau-2\pi/\omega}^{\tau} V_o t \delta_x(t) \frac{\partial \bar{F}_z}{\partial z} \Big|_{\substack{x=x(\tau) \\ z=z(\tau)}} dt \quad (3-16)$$

$$\overline{\delta_x F_z} = 0 + \frac{\varepsilon^2 \pi}{\omega} \frac{\partial \bar{F}_z}{\partial x} \Big|_{\substack{x=x(\tau) \\ z=z(\tau)}} - \frac{2\pi\varepsilon}{\omega^2} V_o \frac{\partial \bar{F}_z}{\partial z} \Big|_{\substack{x=x(\tau) \\ z=z(\tau)}} \quad (3-17)$$

The first term in the above equation vanishes when integrated over one perturbation, and the second term provides the gradient $\frac{\partial \bar{F}_z}{\partial x}$ multiplied by a known constant $\varepsilon^2 \pi$. The third term can be interpreted as an offset due to the motion in the z direction. The offset, however, can be made negligibly small by increasing the perturbation frequency ω and decreasing the insertion speed, since it is inversely proportional to ω^2 and proportional to V_o . In order to correctly estimate the gradient $\frac{\partial \bar{F}_z}{\partial x}$ from correlation $\overline{\delta_x F_z}$, this offset must

be negligibly small. The perturbation frequency ω and the insertion speed must be determined so as to meet this requirement.

3.5 Simulation

In the previous section, eq. (3-17) shows the offset terms related with several variables. This tells how to select the parameters, such as frequency and amplitude of the perturbation and the insertion speed. To verify this condition, several simulations were done with different parameters.

We have obtained the force profile of F_z as a function of x and z as shown in Figure 3-5. This mapping was used for the simulation. Four different conditions are shown in Table 3-1.

	Case 1	Case 2	Case 3	Case 4
Perturbation Amplitude, ϵ	1 [mm]	10[mm]	10 [mm]	1 [mm]
Perturbation Frequency, ω	2 [Hz]	2 [Hz]	20 [Hz]	20 [Hz]
Insertion Speed, V_z	20 [mm/sec]	10 [mm/sec]	20 [mm/sec]	10 [mm/sec]
Proportional Constant, η	0.01	0.01	0.001	0.001

Table 3-1. Conditions for Simulation

The simulation results in Figure 3-10 show that the important factors are the proportional constant and the perturbation frequency. If the perturbation frequency is too low, then, our assumption that the other parameters are constant for one period of perturbation is not valid. For the proportional constant, it is directly related with the stability of the gradient

descent algorithm. This stability is discussed in chapter 4. The magnitude of the offset term is estimated for the real experiment in chapter 5.

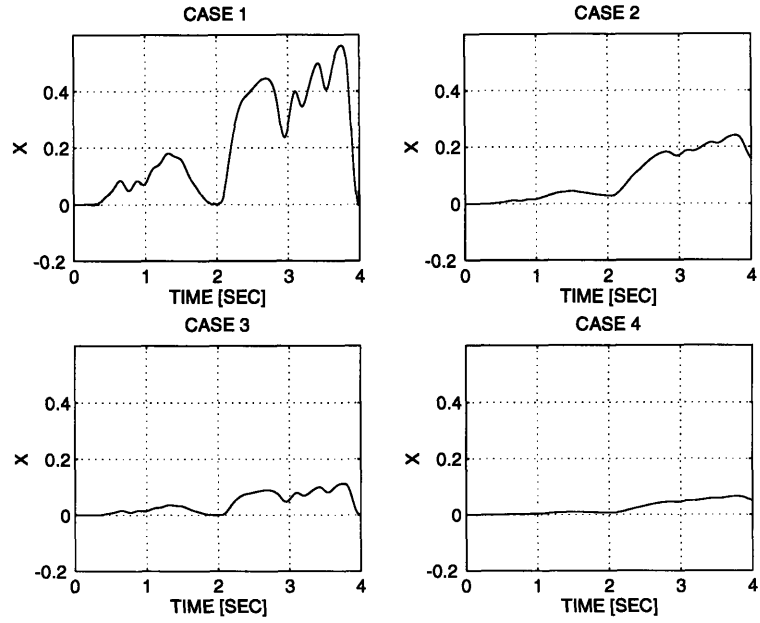


Figure 3-10. Simulation Result

3.6 Extension to Three Dimension

We can extend this example to the three dimensional case. In previous analysis, we assumed that the pipe insertion task is two mensional. In three dimensions, we have one more input variable y , to the performance index F_z , and perturbing both x and y directions, orthogonally, as in eq. (3-18) and (3-19)

$$\delta_x(t) = \epsilon_x \sin \omega t \tag{3-18}$$

$$\delta_y(t) = \epsilon_y \cos \omega t \tag{3-19}$$

Similar analysis would be done as in chapter 3. First, F_z is expanded as :

$$F_z[x(\tau + \Delta t), y(\tau + \Delta t), z(\tau + \Delta t), V_o] =$$

$$F_z[x(\tau), y(\tau), z(\tau), V_o] + \delta_x(t) \frac{\partial F_z}{\partial x} \Big|_{\substack{x=x(\tau) \\ y=y(\tau) \\ z=z(\tau)}} + \delta_y(t) \frac{\partial F_z}{\partial y} \Big|_{\substack{x=x(\tau) \\ y=y(\tau) \\ z=z(\tau)}} + \delta_z(t) \frac{\partial F_z}{\partial z} \Big|_{\substack{x=x(\tau) \\ y=y(\tau) \\ z=z(\tau)}} \quad (3-20)$$

Correlating F_z and δ_x , and taking average for one period of perturbation : $[0, \frac{2\pi}{\omega}]$, we

obtain

$$\overline{\delta_x F_z} \approx \int_{\tau-2\pi/\omega}^{\tau} F_z \Big|_{\tau} \delta_x(t) dt + \int_{\tau-2\pi/\omega}^{\tau} \frac{\partial F_z}{\partial x} \Big|_{\tau} \delta_x(t)^2 dt + \int_{\tau-2\pi/\omega}^{\tau} \frac{\partial F_z}{\partial y} \Big|_{\tau} \delta_x(t) \delta_y(t) dt + \int_{\tau-2\pi/\omega}^{\tau} V_o t \delta_x(t) \frac{\partial F_z}{\partial z} \Big|_{\tau} dt \quad (3-21)$$

with eq. (3-18) and (3-19), eq. (3-21) becomes

$$\overline{\delta_x F_z} = \epsilon_x^2 \pi \frac{\partial \overline{F_z}}{\partial x} \Big|_{\tau} - \frac{2\pi \epsilon_x}{\omega^2} V_o \frac{\partial \overline{F_z}}{\partial z} \Big|_{\tau} \quad (3-22)$$

and also correlating F_z and δ_y , and taking average, we obtain

$$\overline{\delta_y F_z} \approx \int_{\tau-2\pi/\omega}^{\tau} F_z \Big|_{\tau} \delta_y(t) dt + \int_{\tau-2\pi/\omega}^{\tau} \frac{\partial F_z}{\partial x} \Big|_{\tau} \delta_x(t) \delta_y(t) dt + \int_{\tau-2\pi/\omega}^{\tau} \frac{\partial F_z}{\partial y} \Big|_{\tau} \delta_y(t)^2 dt + \int_{\tau-2\pi/\omega}^{\tau} V_o t \delta_y(t) \frac{\partial F_z}{\partial z} \Big|_{\tau} dt \quad (3-23)$$

Again, with eq. (3-18) and (3-19), eq. (3-23) becomes

$$\overline{\delta_y F_z} = \epsilon_y^2 \pi \frac{\partial \overline{F_z}}{\partial y} \Big|_{\tau} \quad (3-24)$$

Note that we the offset term only in eq. (3-22). Table 3-2. shows the comparison between the 2D and the 3D analysis.

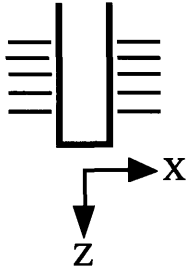
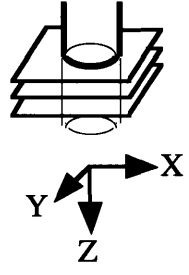
	2D	3D
<i>Coordinate</i>		
<i>Performance Index</i>	$F_z = F_z(x, z, \dot{z})$	$F_z = F_z(x, y, z, \dot{z})$
<i>Perturbation</i>	$\delta_x(t) = \epsilon \sin \omega t$	$\delta_x(t) = \epsilon_x \sin \omega t$ $\delta_y(t) = \epsilon_y \cos \omega t$
V_z	V_o	V_o
<i>Control Law</i>	$x_d = x_o - \eta \int_0^t \frac{\partial F_z}{\partial x} d\tau$	$x_d = x_o - \eta \int_0^t \frac{\partial F_z}{\partial x} d\tau$ $y_d = y_o - \eta \int_0^t \frac{\partial F_z}{\partial y} d\tau$

Table. 3-2

Simulation was done for this case. Figure 3-11 shows the trajectory time history, and Figure 3-12 shows the performance index, F_z .

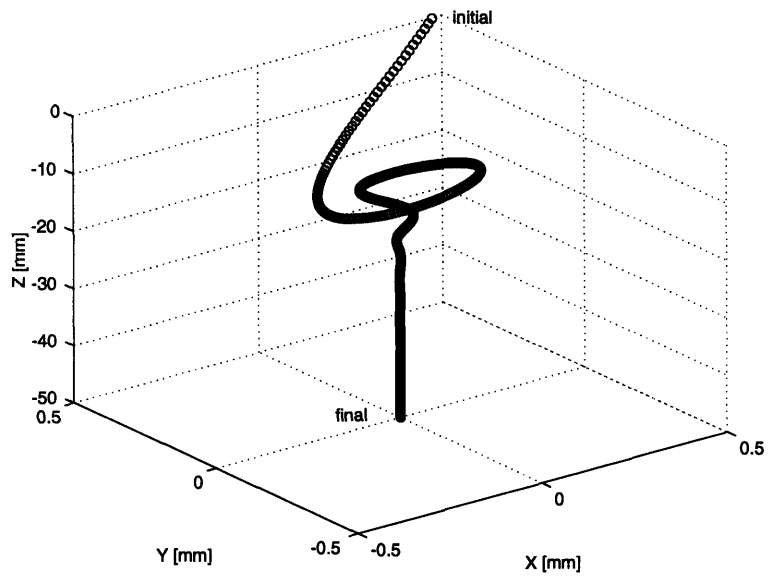


Figure 3-11. End Effector Trajectory

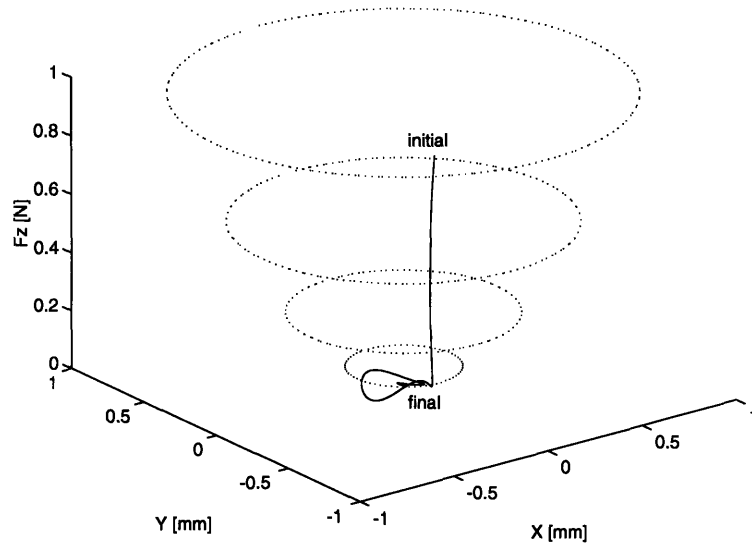


Figure 3-12. Performance Index Time History

We have shown that this controller can be used for three dimensional case by simulation.

4.1 Introduction

In the previous chapter, we have developed a model of the pipe insertion task. Based on this model, we need to check the stability of the whole system. We get a linear system model including the perturbation/correlation part, however, we still don't have exact model of the performance index, which is F_Z . This is actually unknown and can not be represented exactly by mathematical expression. We assumed that it has a parabolic form, and has a minimum point. From the experimental data, we verified that our assumption is correct, but still its exact shape is not known, which depends on the holes and many other characteristics. We start from a simple parabolic form of F_Z so that the whole system becomes linear. In the following section, we get the stability boundary by applying Popov theorem even though the performance index is not known and nonlinear.

4.2. Linear System

Based on system model in the previous section, we check the stability of the system based on Routh's stability criterion. Consider the perturbation/correlation based system shown in Figure 4-1.

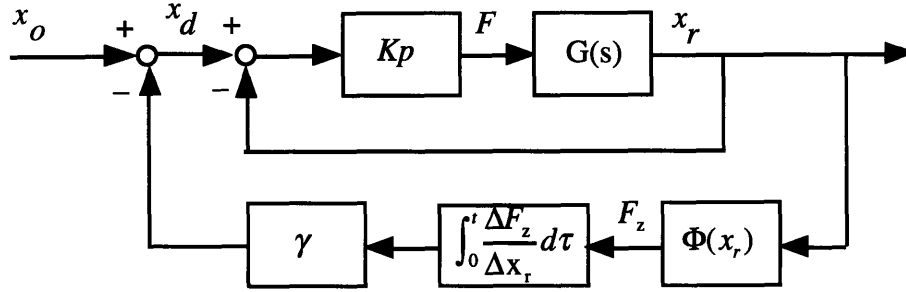


Figure 4-1. Block diagram representation

For simplicity, let's assume the F_z is a parabolic function as in eq. (4-1)

$$F_z = \frac{1}{2}ax_1^2 + c \quad (4-1)$$

where, $a > 0$

we have the transfer function of the system as in eq. (4-2)

$$G(s) = \frac{1}{ms^2 + bs + K_e} \quad (4-2)$$

and the trajectory command is updated based on eq. (4-3)

$$x_d = x_o - \gamma \int_0^t \frac{\Delta F_z}{\Delta x_r} d\tau \quad (4-3)$$

where, γ is a positive update constant and the initial nominal trajectory x_o is usually zero.

To represent this system in a state space form, let

$$\dot{x}_1 = x_2 \quad (4-4)$$

$$\dot{x}_2 = -\frac{K_e + K_p}{m}x_1 - \frac{b}{m}x_2 - \gamma \frac{K_p}{m}x_3 \quad (4-5)$$

$$\dot{x}_3 = \frac{\partial F_z}{\partial x_1} \quad (4-6)$$

with eq. (4-1), eq. (4-6) becomes

$$\dot{x}_3 = ax_1 \quad (4-7)$$

The system's state equations are given by,

$$\begin{pmatrix} \dot{x}_1 \\ \dot{x}_2 \\ \dot{x}_3 \end{pmatrix} = \begin{bmatrix} 0 & 1 & 0 \\ -\frac{K_e + K_p}{m} & -\frac{b}{m} & -\gamma\frac{K_p}{m} \\ a & 0 & 0 \end{bmatrix} \begin{pmatrix} x_1 \\ x_2 \\ x_3 \end{pmatrix} \quad (4-8)$$

and the characteristic equation is,

$$ms^3 + bs^2 + (K_p + K_e)s + \gamma a K_p = 0 \quad (4-9)$$

From Routh's stability criterion, we get stability condition as in eq. (4-10)

$$0 < \gamma < \frac{b(K_e + K_p)}{amK_p} \quad (4-10)$$

4.3 Nonlinear and Unknown System

The stability analysis in the previous section was done using Routh's stability criterion, but that was based on the assumption that the nonlinearity has a parabolic form, so that we can transform the system into a linear one. However, in the real assembly task, this displacement-to-force map is not well known. To be more practical, we need to find out the conditions of the stability not only for the parameter values in the controller, but also the characteristics of the nonlinearity. We are applying Povpov criterion for this purpose.

In the system considered in Figure 4-2, the forward path is a linear time-invariant system, and the feedback part is a nonlinear static mapping.

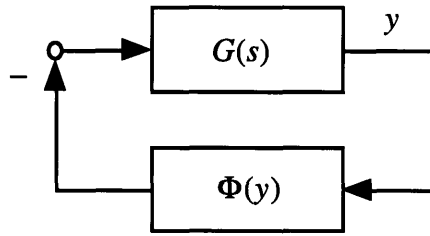


Figure 4-2. System with nonlinearity

The equation of this system can be represented as,

$$\dot{X} = AX - B\Phi(y) \quad (4-11)$$

$$y = CX \quad (4-12)$$

$$G(s) = C[sI - A]^{-1} B \quad (4-13)$$

where, Φ is a nonlinear function. To check the stability of this system, Popov criterion imposes several conditions for asymptotic stability.

Conditions

- A has all the eigenvalues with non positive real parts but with only a simple zero eigenvalue.
- (A,B) is controllable
- (A,C) is observable
- Nonlinearity Φ belongs to a sector $[0,K]$
- there exists a strictly positive number α , such that

$$\forall \omega \geq 0, \operatorname{Re}[(1 + j\alpha\omega)G(j\omega)] + \frac{1}{K} \geq \epsilon \quad (4-14)$$

for an arbitrarily small $\epsilon > 0$, then, the point 0 is globally asymptotically stable.

let $G(j\omega) = G_1(j\omega) + jG_2(j\omega)$, then,

$$G_1(j\omega) - \alpha\omega G_2(j\omega) + \frac{1}{K} \geq \epsilon \quad (4-15)$$

For the nonlinear function in our system, let's assume that there is an unknown nonlinearity mapping which belongs to a sector $[0, K]$ as in Figure 4-3.

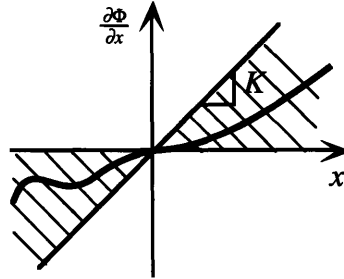


Figure 4-3. Nonlinearity

then, the mapping between the robot displacement x_r and the force in the z -direction, F_z , would be as in Figure 4-4.

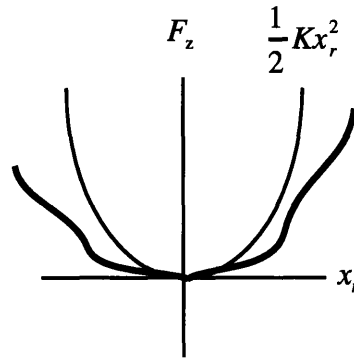


Figure 4-4. Displacement vs. Force

Now, for stability analysis, we need to know only the upper bound of K in Figure 4-3, not the exact shape of the nonlinearity. To represent this system in a state space form, let

$$\dot{x}_1 = x_2 \quad (4-16)$$

$$\dot{x}_2 = -\frac{K_e + K_p}{m} x_1 - \frac{b}{m} x_2 - \gamma \frac{K_p}{m} x_3 \quad (4-17)$$

$$\dot{x}_3 = \Phi(x_1) = \frac{\partial F_z}{\partial x_1} \quad (4-18)$$

$$A = \begin{bmatrix} 0 & 1 & 0 \\ -\frac{K_e + K_p}{m} & -\frac{b}{m} & -\gamma\frac{K_p}{m} \\ 0 & 0 & 0 \end{bmatrix} \quad (4-19)$$

$$B = \begin{bmatrix} 0 \\ 0 \\ -1 \end{bmatrix} \quad (4-20)$$

$$C = [1 \ 0 \ 0] \quad (4-21)$$

and check the condition of Popov stability,

- eigenvalues of A

$$\left\{ 0, \frac{-b \pm \sqrt{b^2 - 4m(K_e + K_p)}}{2m} \right\}$$

- (A,B) is controllable
- (A,C) is observable

Now for graphical interpretation, the system transfer function of the linear part is,

$$G(s) = \frac{\gamma K_p}{ms^3 + bs^2 + (K_e + K_p)s} \quad (4-22)$$

$$G(j\omega) = \frac{\gamma K_p}{-b\omega^2 + j[-m\omega^3 + (K_e + K_p)\omega]} \quad (4-23)$$

$$G(j\omega) = \frac{-b\gamma K_p \omega^2 + j[m\omega^3 - (K_e + K_p)\omega]}{b^2 \omega^4 + [-m\omega^3 + (K_e + K_p)\omega]^2} \quad (4-24)$$

the real part of $G(j\omega)$ is

$$\operatorname{Re}[G(j\omega)] = \frac{-b\gamma K_p \omega^2}{b^2 \omega^4 + [-m\omega^3 + (K_e + K_p)\omega]^2} \quad (4-25)$$

and the imaginary part of $G(j\omega)$ is

$$\operatorname{Im}[G(j\omega)] = \frac{m\omega^3 - (K_e + K_p)\omega}{b^2 \omega^4 + [-m\omega^3 + (K_e + K_p)\omega]^2} \quad (4-26)$$

let's define

$$\operatorname{Im}[G^*(j\omega)] = \omega \operatorname{Im}[G(j\omega)] \quad (4-27)$$

then,

$$\operatorname{Im}[G^*(j\omega)] = \frac{m\omega^4 - (K_e + K_p)\omega^2}{b^2 \omega^4 + [-m\omega^3 + (K_e + K_p)\omega]^2} \quad (4-28)$$

to plot eq. (4-25) and eq. (4-28) on $\operatorname{Re}[G(j\omega)]$ and $\operatorname{Im}[G^*(j\omega)]$ plane, we need to check several points. First of all, for $\omega = 0$

$$\operatorname{Re}[G(j\omega)] = -\frac{b\gamma K_p}{(K_e + K_p)^2} \quad (4-29)$$

$$\operatorname{Im}[G^*(j\omega)] = -\frac{1}{K_e + K_p} \quad (4-30)$$

for $\omega = \infty$

$$\operatorname{Re}[G(j\omega)] = 0 \quad (4-31)$$

$$\operatorname{Im}[G^*(j\omega)] = 0 \quad (4-32)$$

for $\operatorname{Im}[G^*(j\omega)] = 0$

$$\omega_o = \sqrt{\frac{K_e + K_p}{m}} \quad (4-33)$$

for $\omega = \omega_o$

$$\operatorname{Re}[G(j\omega_o)] = -\frac{\gamma m K_p}{b(K_e + K_p)} \quad (4-34)$$

and finally to get the slope,

$$\frac{\partial \operatorname{Im}[G^*(j\omega)]}{\partial \operatorname{Re}[G(j\omega)]} = \frac{\partial \operatorname{Im}[G^*(j\omega)]}{\partial \omega} \frac{\partial \omega}{\partial \operatorname{Re}[G(j\omega)]} = \frac{\partial \operatorname{Im}[G^*(j\omega)] / \partial \omega}{\partial \operatorname{Re}[G(j\omega)] / \partial \omega} \quad (4-35)$$

$$\frac{\partial \text{Im}[G^*(j\omega)]}{\partial \text{Re}[G(j\omega)]} = \frac{(K_e + K_p)b^2 - (K_e + K_p)^2 m + 2(K_e + K_p)m^2 \omega^2 - m^3 \omega^4}{bK_p \gamma [b^2 - 2(K_e + K_p)m + 2m^2 \omega^2]} \quad (4-36)$$

the slope for $\omega = 0$

$$\frac{\partial \text{Im}[G^*(0)]}{\partial \text{Re}[G(0)]} = \frac{(K_e + K_p)[b^2 - (K_e + K_p)m]}{bK_p \gamma [b^2 - 2(K_e + K_p)m]} \quad (4-37)$$

and for $\omega = \omega_o$,

$$\frac{\partial \text{Im}[G^*(j\omega_o)]}{\partial \text{Re}[G(j\omega_o)]} = \frac{(K_e + K_p)}{\gamma b K_p} \quad (4-38)$$

the complete plot of this transfer function is shown in Figure 4-5.

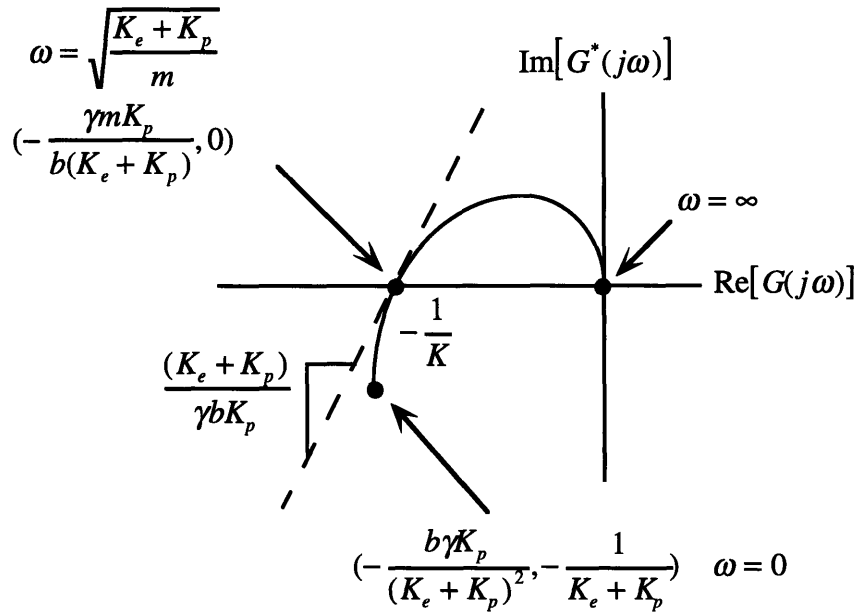


Figure 4-5. Plot of transfer function

From Figure 4-5, we can see the system is stable because there exists a positive number α , such that

$$\frac{1}{\alpha} = \frac{(K_e + K_p)}{\gamma b K_p} > 0 \quad (4-39)$$

and if the following condition is satisfied,

$$-\frac{1}{K} < -\frac{\gamma m K_p}{b(K_e + K_p)} \quad (4-40)$$

Therefore, the system is stable when,

$$\gamma < \frac{b(K_e + K_p)}{m K_p K} \quad (4-41)$$

Comparing eq. (4-41) with eq. (4-10) in the linear case, both are the same, but this Popov criterion is based on sector nonlinearity, of which the shape of the nonlinearity is not known exactly. Therefore, once we get the maximum value of slope in the sector, we can get the stability condition even though there exists an unknown nonlinearity.

4.4 Simulation

To verify the stability condition of eq. (4-10), let us choose the following parameter values based on the estimation of the real system.

$$m = 0.042 \text{ [Kg]}$$

$$b = 2.1 \text{ [Nsec/m]}$$

$$K_e = 133 \text{ [N/m]}$$

$$K_p = 100$$

and for simplicity, let's assume the nonlinearity is a parabolic form of

$$a = 0.5$$

then, the maximum value of the proportional constant in the update law is,

$$\gamma_{\max} = \frac{b(K_e + K_p)}{amK_p} = 58.25$$

and F_z is calculated on,

$$F_z = \frac{1}{2}ax_1^2 \quad (4-42)$$

The following four cases show the trajectory of the system with different initial conditions and different values of update constant, γ .

Case 1

$$\text{initial condition : } X_o = \begin{pmatrix} 1 \\ 0 \\ 0 \end{pmatrix} \quad \text{update constant : } \gamma = 0.25\gamma_{\max}$$

Case 2

$$\text{initial condition : } X_o = \begin{pmatrix} -1 \\ 0 \\ 0 \end{pmatrix} \quad \text{update constant : } \gamma = 0.25\gamma_{\max}$$

Case 3

$$\text{initial condition : } X_o = \begin{pmatrix} 1 \\ 0 \\ 0 \end{pmatrix} \quad \text{update constant : } \gamma = \gamma_{\max}$$

Case 4

$$\text{initial condition : } X_o = \begin{pmatrix} 1 \\ 0 \\ 0 \end{pmatrix} \quad \text{update constant : } \gamma = 1.5\gamma_{\max}$$

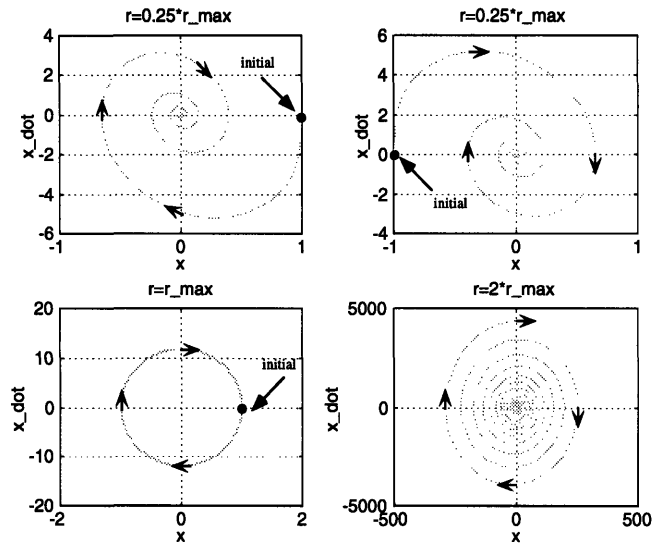


Figure 4-6. Simulation Results for Linear Case

Figure 4-6 verifies the stability analysis in section 4.2. For case 1 and case 2, the system is stable regardless of the initial condition. For case 3, the system is marginally stable with maximum value of update constant. The system diverges with larger value than the maximum update constant in case 4.

In order to verify the condition for the nonlinear case, a random force function which belongs to the sector $[0,1]$ is generated as shown in Figure 4-7.

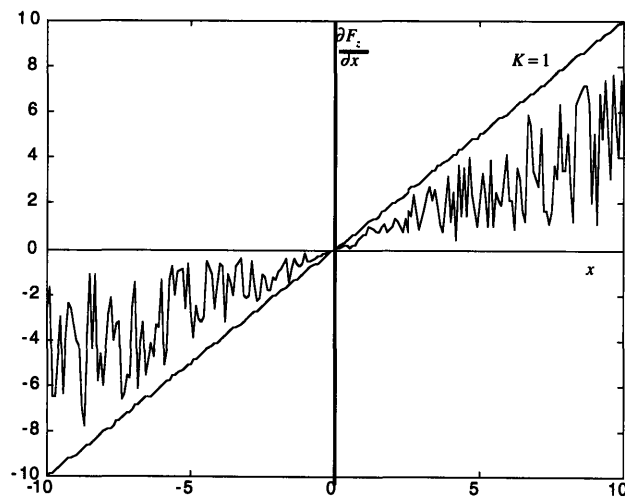


Figure 4-7. Nonlinear Force Function

Similar simulations were performed based on this nonlinear force function. The result is shown in Figure 4-8.

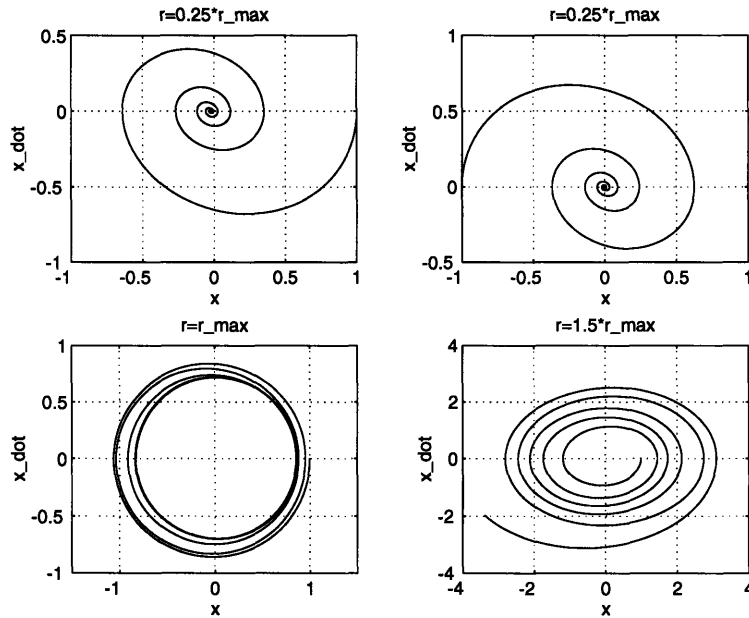


Figure 4-8. Simulation Results for Nonlinear Case

The Popov stability criterion is more conservative than the linear case, so even with the maximum value of the gain, the system converges. Therefore, once we found a sector the nonlinear function belongs to, we can calculate the maximum stable gain. With the real experimental data obtained in chapter 3., we have the sector value of the nonlinearity in our system. One conservative estimate is,

$$K = 2 \times 10^7 \text{ [N/mm}^2\text{]}$$

and then, the maximum proportional feedback gain is,

$$\gamma_{max} = 5.825 \times 10^{-6}$$

Therefore, we selected a feedback gain less than this maximum value for the experiment.

Chapter 5

Experiment and Implementation

5.1 Introduction

We have generalized the perturbation/correlation based control, and for case study, we selected the pipe insertion task in the chapter 3 and did stability analysis in chapter 4. In this chapter, we implemented this pipe insertion task using robot. To generate high frequency perturbation, we designed and implemented a vibratory end effector. With this end effector attached to the end of the robot, this task was done using three axis robot. First, the vibratory end effector was described, followed by the experimental setup. The experimental results were shown and compared with other force guided controllers.

5.2 Vibratory End Effector Using Piezo Electric Actuator

In chapter 2, we mentioned that high frequency perturbation with negligible phase is required for stability. To satisfy this requirement, we use a piezo electric actuator. The piezo electric actuator has a very high bandwidth. We are using this actuator to generate high frequency vibration with negligible phase lag. However, another characteristic of the piezo actuator is the displacement is very small even though the force generated is quite large. We need a device to amplify the displacement. The specifications of the actuator used are as follows.

- Bandwidth > 50 [Hz]

- Force : 3.2 [kN]
- Displacement : 80 [μm]

Due to the geometric constraint of the assembly system, we need about 1 mm amplitude of vibration. It is hard to generate this small amplitude of vibration just using robot body. This vibratory endeffector is a very good solution to this requirement for high frequency and small amplitude vibration. With the vibratory endeffector and pipe, amplification of 13 times is possible which satisfies the requirement. Figure 5-1 shows the draft of the endeffector.

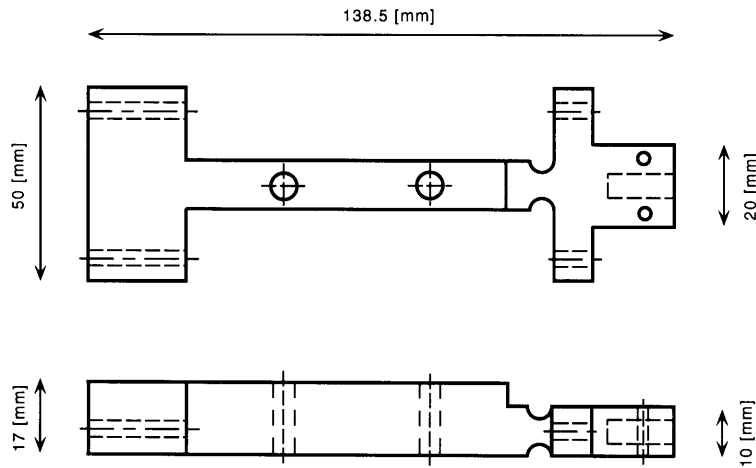


Figure 5-1. Vibratory Endeffector

Two piezo electric actuators are pushing/pulling the head to generate rotational movement of the head as in Figure 5-2. A notch is made on both sides to give a pivoting point.

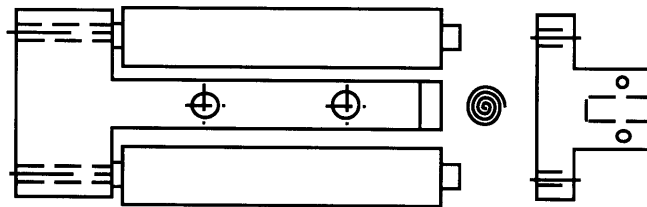


Figure 5-2. Isolated view of the End Effector Head

This notch works as a rotational joint, with stiffness, and force is given from the actuators. The head of the end effector is rotating, and the other end of the copper pipe is generating amplified displacement.

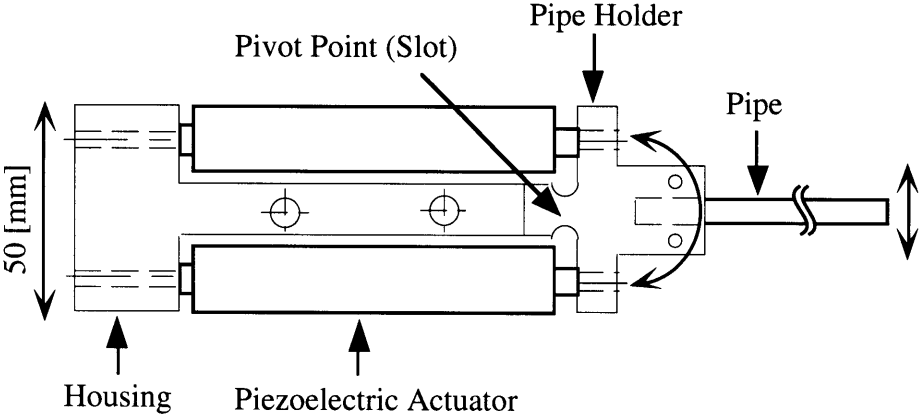


Figure 5-3. Movement of the End Effector

The real vibratory end effector is shown in Figure 5-4.

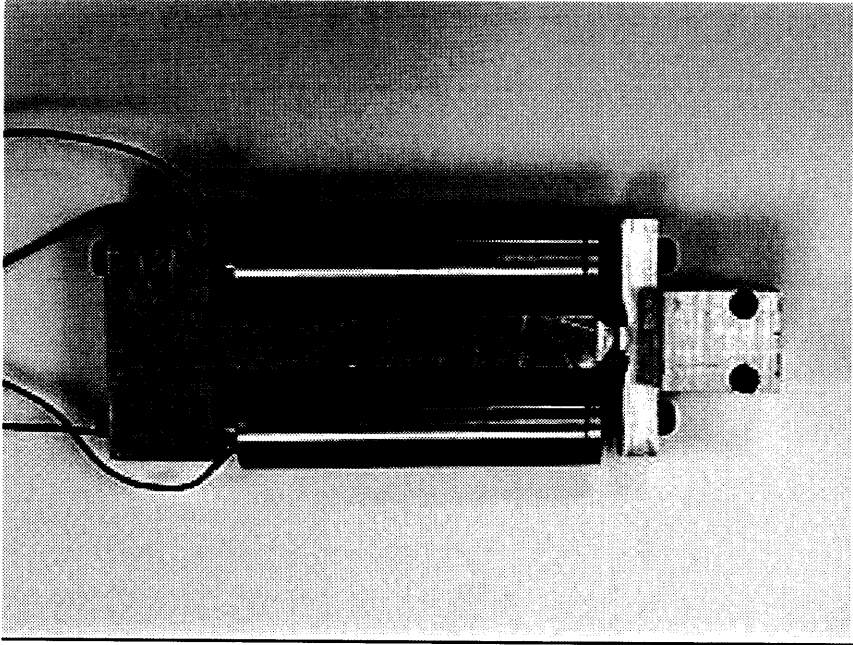


Figure 5-4. Vibratory End Effector with Piezo Electric Actuators.

5.3 Experimental Setup

We implemented the perturbation/correlation based controller for the insertion of a long copper pipe into a heat exchanger. A three degree of freedom robot is controlled by a Sun Work Station with VxWorks real time operating system. The sampling time of the control system is 1 ms. The force sensor is mounted between the arm's endpoint and the vibratory endeffector as shown in Figure 5-5.

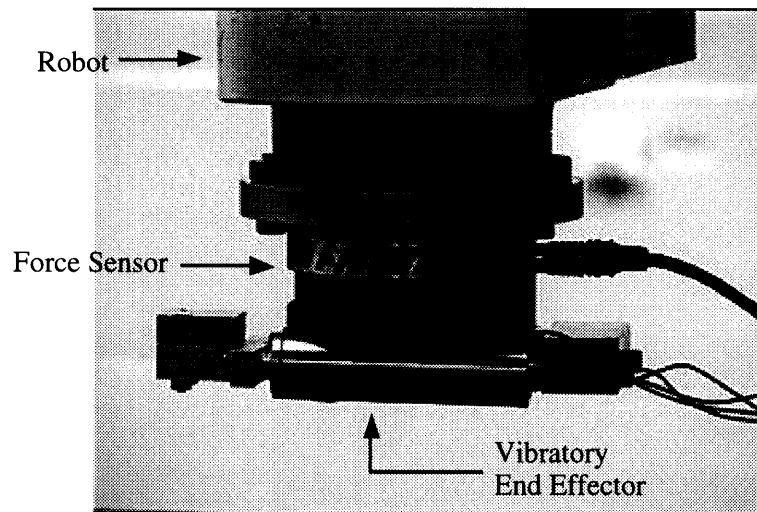


Figure 5-5. Vibratory End Effector Mounted on a Force Sensor

The diameter of the pipe is 8mm, the clearance is about 0.01, and aluminum foils are stuck for inserting the pipe. The required insertion depth is 500mm. Figure 5-6 shows the experimental setup. This piezo-electric actuators are controlled independently with the perturbation/correlation based controller. A sinusoidal displacement command was given to these actuators, but the force response due to this perturbation input is used to calculate the gradient value of the performance index. This open loop controller for piezo electric actuator followed the desired sinusoidal trajectory command with negligible phase lag, which is important to get the correct gradient information. The three axis of the robot were

controlled independently using PID controllers. At every sampling time, the desired joint angles were calculated from inverse kinematics routine, based on the desired positions in Cartesian coordinates.

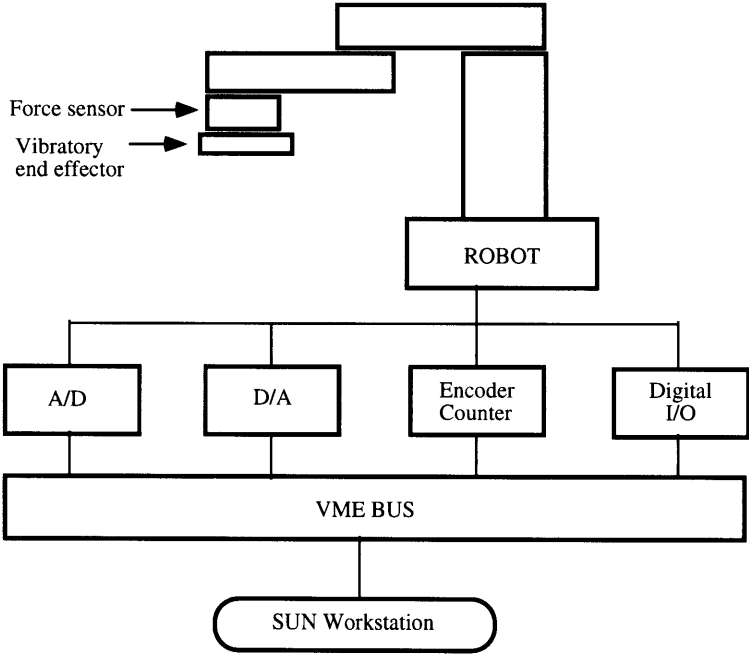


Figure 5-6. Experimental Setup

The robot inserts a copper pipe into the heat exchanger as shown in Figure 5-7.

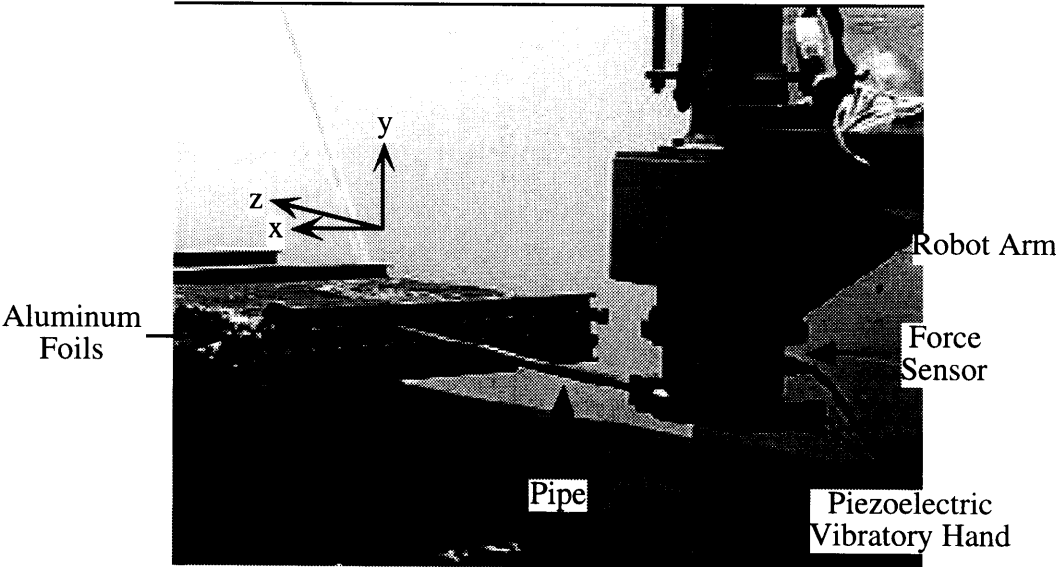


Figure 5-7. Pipe Insertion by Robot

5.4 Experimental Data

Figure 5-8 shows the time profiles of the robot motion of x direction, the insertion direction of z , the response force, F_x and the obstructing force F_z . The vibratory endeffector was perturbed with 20 Hz in frequency. For the following one period, the correlation was evaluated. In proportion to the resultant correlation \hat{R}_x , the x axis command was corrected.

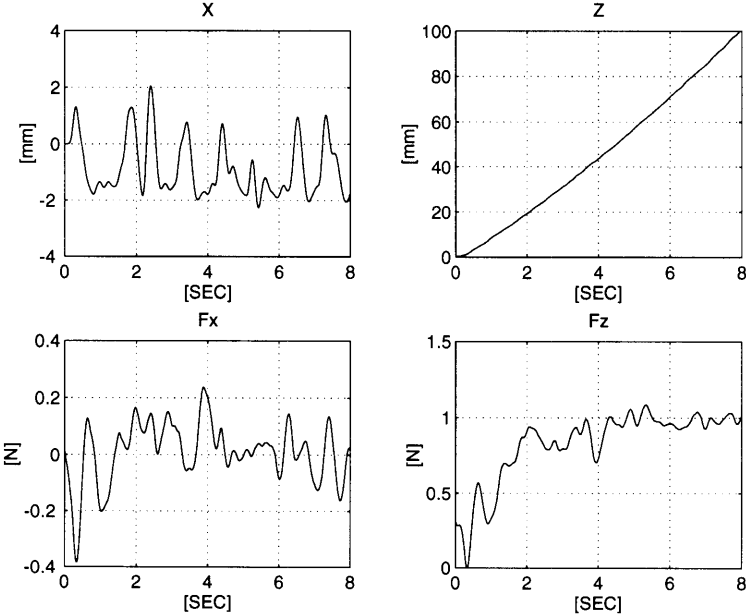


Figure 5-8. Experimental Data

The x directional reference trajectories are changed in real time based on correlation value. While generating perturbation, the input to the environment (position perturbation) and the performance index of the system (F_z) are calculated according to the correlation equation. Finally, the correlation value is used for updating the trajectory command. For this experiment we focused only on minimizing the force in the z -direction.

In chapter 3, a condition was derived for the validity of perturbation/correlation as in eq.

(5-1).

$$\overline{\delta_x F_z} = \frac{\epsilon^2 \pi}{\omega} \frac{\partial F_z}{\partial x} \Big|_{\substack{x=x(\tau) \\ z=z(\tau)}} - \frac{2\pi\epsilon}{\omega^2} V_o \frac{\partial F_z}{\partial z} \Big|_{\substack{x=x(\tau) \\ z=z(\tau)}} \quad (5-1)$$

To satisfy this condition, we use a small value of V_z and a high frequency of perturbation ω . However, it is necessary to verify this condition based on our experimental data. We calculate the value of $\overline{\delta_x F_z}$ on real time and use that value to update the trajectory command. We have the values of $\overline{\delta_x F_z}$ saved during the experiment. We can't get exact value of $\frac{\partial F_z}{\partial x}$ but we are estimating from $\overline{\delta_x F_z}$. In the chapter 3, we showed the measured value of F_z without perturbation, so we also get estimate of $\frac{\partial F_z}{\partial z}$. By comparing the magnitude of $\overline{\delta_x F_z}$ and $\frac{2\pi\epsilon V_o}{\omega^2} \frac{\partial F_z}{\partial z}$, we can validate our assumption. Figure 5-9 shows the values of these two under the same condition, which is with the same V_z . We can see clearly that $\overline{\delta_x F_z}$ is more than 1000 times larger than $\frac{2\pi\epsilon V_o}{\omega^2} \frac{\partial F_z}{\partial z}$, therefore the offset due to the second term is negligible.

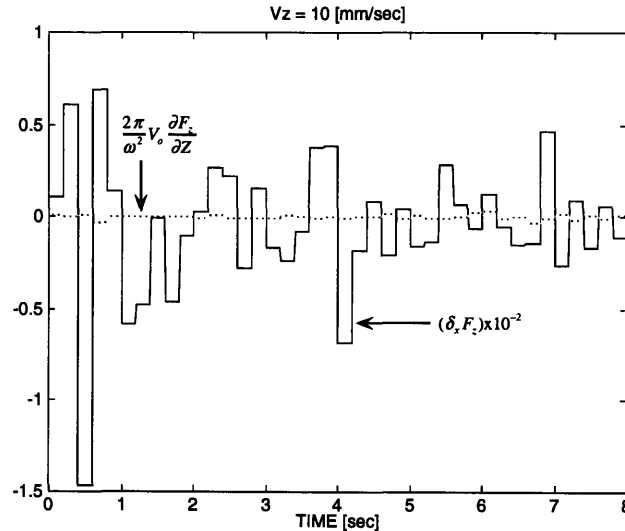


Figure 5-9. Verification of the Eq (5-1)

5.5 Comparison with Other Force-Guided Controller

There exist many force-guided controller developed and some of them are good for specific tasks. We need to compare the performance of this correlation/perturbation based controller with other force-guided controllers. One of the common controller is the compliance controller. Also, in order to check the improvement of using this vibratory end effector, we compare with the same perturbation/correlation based controller but generating dither by shaking the robot arm.

For the peg-in-hole insertion task, the conventional compliance controller works fine. This controller is based on desired compliance characteristics at the entrance of the hole and implementing joint compliance controller. However, for this pipe insertion case, the local force information is not informative enough to guide the pipe passively and the insertion depth is much larger. A compliance controller is designed to place the desired compliance center at the tip of the copper pipe as in Figure 5-10.

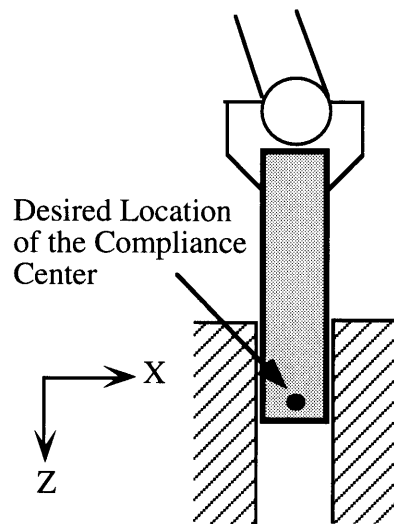


Figure 5-10. Compliance Center

with the following compliance values at the location of the compliance center.

$$C_c = \begin{bmatrix} c_{xx} & 0 & 0 \\ 0 & c_{zz} & 0 \\ 0 & 0 & c_{\theta\theta} \end{bmatrix} \quad (5-2)$$

$$c_{xx} = 0.1 \text{ [m/N]}$$

$$c_{zz} = 0.001 \text{ [m/N]}$$

$$c_{\theta\theta} = 0.02 \text{ [rad/Nm]}$$

The force response of this compliance controller is shown in Figure 5-12 with other controllers. Another force guided control [Lee, Asada-1 1995] is by generating dither using the robot body. Due to the bandwidth of the robot and its controller, we are not able to get a high frequency dither. Therefore, the trajectory update is slower than this new method. Figure 5-11 shows the trajectory of the robot and the resistant force. The position of the robot arm is controlled based on the updated trajectory command and also perturbed sinusoidally as well by adding sinusoidal displacement command.

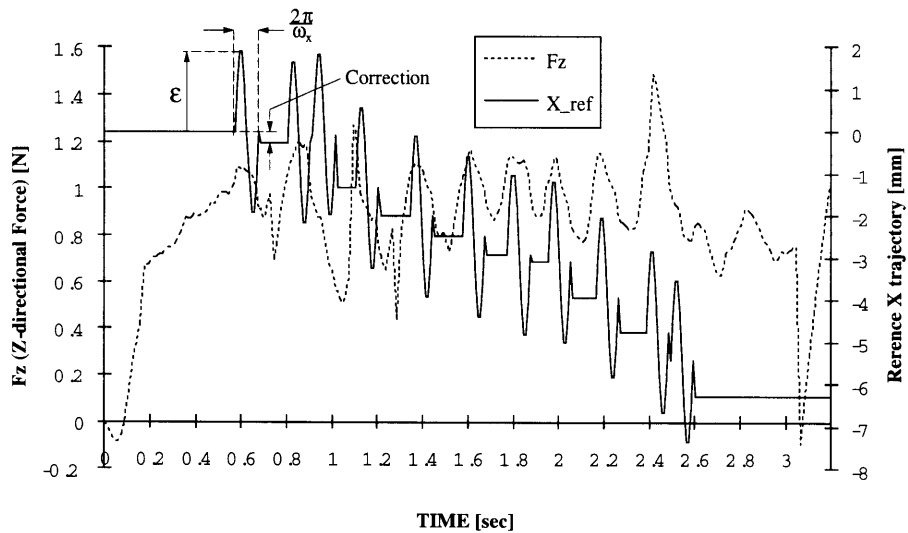


Figure 5-11. X-displacement and Force Response of the Robot Dither Case

For the above experiment, a dither frequency of 5Hz was used. The other conditions such as insertion velocity, depth are the same as the one with vibratory end effector, but the amplitude of the dither was 2mm. The x-trajectory shown in Figure 5-11 is a given trajectory command. The comparison with those two other methods is shown in Figure 5-12. This clearly shows the effectiveness of this method.

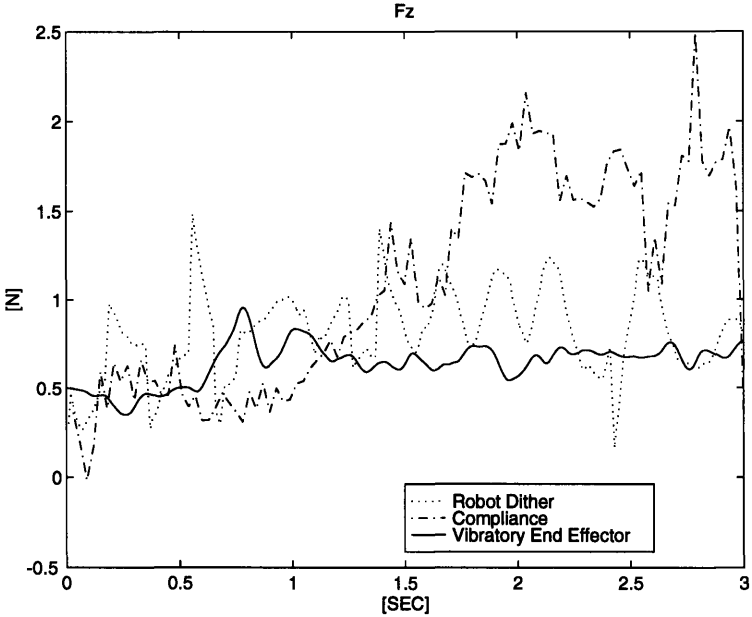


Figure 5-12. Comparison with Conventional Controller

5.6 Friction Reduction Due to Perturbation

In this perturbation/correlation based control, we perturb the displacement input to the system in order to get the gradient of the resistant force. The resistant force is composed of many forces, and one of them is the friction force. The coulomb friction is known to be proportional to the normal force. As we perturb in x-direction, it causes a change in normal force and we expect that this perturbation to help reduce the friction force. To see the effect of the perturbation, we measured the force response in a way similar to the

one in chapter 3. The difference is that we mounted the vibratory end effector on the force sensor so that it generates a perturbation as shown in Figure 5-13.

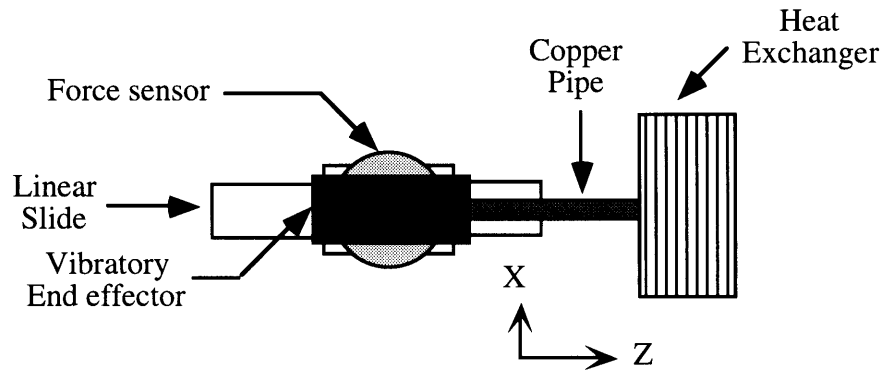


Figure 5-13. Experiment Setup

We measured the force data as we move with constant velocity in the z -direction and repeated several times with different x displacements. Note that the x trajectory is still fixed and we didn't update the trajectory based on the correlation result. This experiment is purely for estimating the effect of perturbation to reduce the friction. Same as before, we obtained similar parabolic shaped force response as shown in Figure 5-14. The magnitude of the resistant force is much smaller than the previous case which is without perturbation. However, this force data still shows that the minimum point of the force is not on fixed point of x , so it is required to adjust x to reduce this force. Also, we don't know exactly where this minimum points lies, so we need to perturb the displacement, and update the trajectory based on the gradient value.

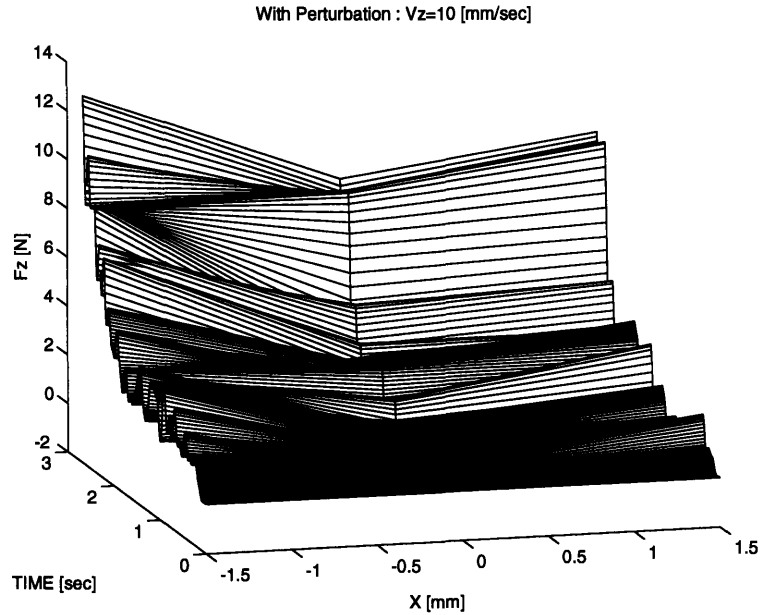


Figure 5-14. Force Profile with Perturbation

Figure 5-15 shows the comparison among these three cases under same condition. First one is the perturbation/correlation based controller, and the second one is with perturbation, and the last one without perturbation. We can see the effect of updating the trajectories based on the correlation value from Figure 5-15. Combining perturbation with trajectory update based on correlation, we could get the best result. In other words, perturbations work both for reducing the friction and estimating the direction to which we should move the pipe in order to reduce the resistant force.

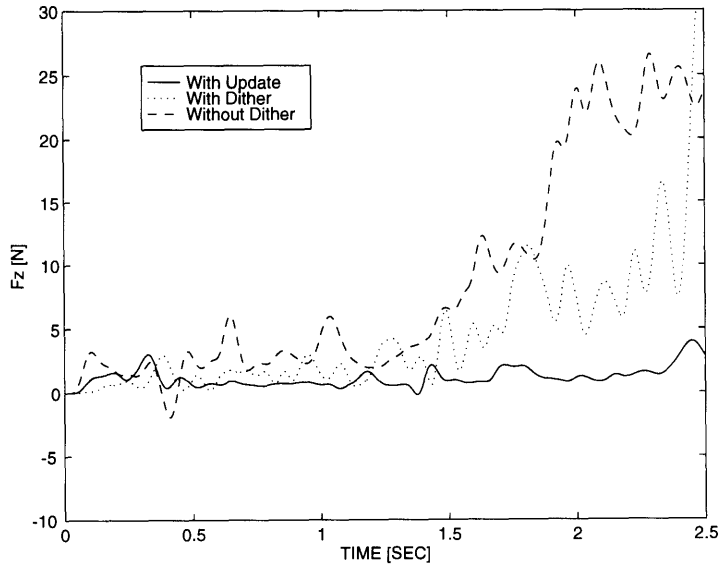


Figure 5-15. Resistant Force Comparison

Chapter 6

Application to the Connector Assembly Task

6.1 Introduction

The perturbation/correlation based control can be applied to other tasks. For a force guided robot assembly, a performance index which represents the characteristics of the task is selected and then a controller is made to minimize this performance index. Force information is very essential to estimate the current state and generate new command. However, the force from the most of the real assembly task is not informative enough to guide the robot to accomplish the task. Especially, when the force to motion mapping is not linear and the environment information is not well known, this perturbation/correlation based control is a good solution. We select the connector assembly task as an example and apply this control algorithm. Through simulation based on the analytical model, we show the effectiveness of this approach. The comparison between this connector assembly task and the previous heat exchanger assembly is discussed at the end.

6.2 Connector Assembly

The control method developed for the above heat exchanger assembly can be applied to a class of tasks, where a workpiece is guided along unknown reference surfaces by maintaining contacts with them. Consider the assembly of connectors shown in Figure 6-1. The typical assembly process shown in the figure can be controlled in the same manner as the heat exchanger assembly. First, the male connector held by a robot is placed on the

female connector as shown in (a), and is rotated while maintaining contacts with the female connector as shown in (b). When the male connector comes into an upright position as shown in (c), it is mated with the female connector and slides into the female connector (d). During this process, the male connector is pushed against the female connector so that the male connector can be guided along the surfaces of the female connector. The force applied to the male connector ensures the mechanical contacts with the reference surface of the female connector. The contact forces should be kept small, since large contact forces create large friction which may incur stick slip when guiding along the contact surfaces. The male connector should gently touch the female connector with small contact forces that ensure the contacts while rotating the male connector.

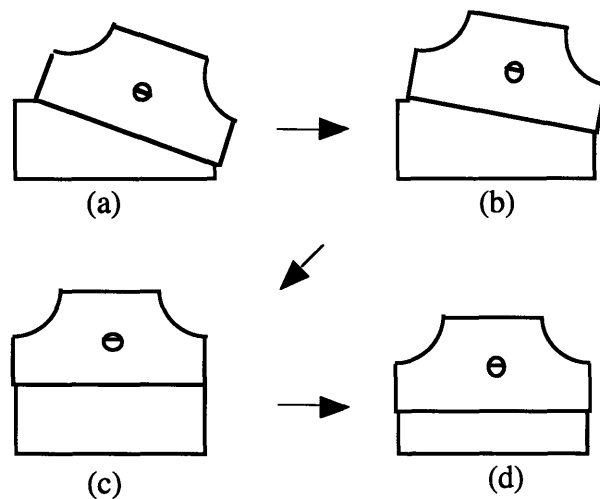


Figure 6-1. Connector Assembly

This control strategy for guiding the male connector can be formulated in the same way as the heat exchanger assembly. The z axis motion in the heat exchanger assembly indicates the depth of insertion, or the progress of assembly, and its speed is controlled with a prescribed time function, typically a constant speed. Likewise, the rotational motion of the male connector indicates the progress of the process, and its angular velocity is controlled with a prescribed time function. In the heat exchanger assembly, the insertion

force F_z was considered as a performance index to minimize. Likewise, the contact force between the male and female connectors can be treated as a type of performance index : the deviation from a desired contact force, which is small, should be minimized during the process. Also, the friction between the two or the moment created by the friction about the center of rotation of the male connector can be used as the performance index. In the heat exchanger assembly, the performance index was minimized by shifting the x position. To obtain the gradient of F_z to x , a perturbation was applied to the x axis and the correlation with F_z was evaluated in order to guide the object to the minimum. Accordingly, the performance index in the connector assembly, i.e. the contact force, is optimized through the accommodation of x and y axes by superimposing perturbations on both axes and evaluating the correlations. To obtain the gradient in both x and y directions, orthogonal perturbations must be given to both axes, as will be shown in the following section.

In the connector assembly, the contact force and friction become large when the male connector is not correctly guided along the reference surfaces of the female connector ; it tends to move into the reference surfaces. Also, when the male connector tends to depart from the reference surfaces, the contact for becomes lower than a specified level. Therefore, force guided assembly in those tasks can be treated as a problem of minimizing a performance index in terms of resistive forces. To guide a workpiece towards the minimum of the performance index, the perturbation and correlation technique can be used as a powerful tool. Despite noisy, erratic force signals, the perturbation/correlation method would be able to guide a workpiece in the direction towards the optimal of a given performance index. In the following section, the proposed method will be formally described.

6.3 Modeling

The connector assembly task illustrated in Figure 6-1 is to correctly mate the male connector to the female connector. Since the location of the female connector is not exactly known, we make the male connector gently touch the female one, pressing it against and rotating until it reaches the upright position. Based on the external forces, the corresponding trajectory command, V_x , V_y and ω_z can be generated based on linear mapping. However, if there exists friction as shown in Figure 6-2, and the friction constant is not known, the mapping is not linear anymore. We are applying the perturbation/correlation based control to this task.

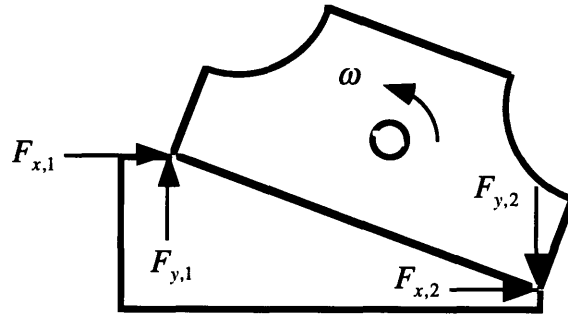


Figure 6-2. Reaction Forces

As mentioned earlier, the force is used for obtaining unknown surface information. The goal of this task is not only assembling the connector, but also maintaining desired contact force. In other words, we need to push the male connector to the female connector not to lose contact, but with minimum force. Because a large normal force to the other connector causes large friction force, thereby, we may have stick-slip and even jamming. Therefore, our performance index is chosen as in eq. (6-3) and our goal is to minimize this performance index while giving constant angular velocity command, ω .

$$F_x = F_{x1} + F_{x2} \quad (6-1)$$

$$F_y = F_{y1} - F_{y2} \quad (6-2)$$

$$P.I. = (F_x - F_{x,o})^2 + (F_y - F_{y,o})^2 \quad (6-3)$$

where, $F_{x,o}$ and $F_{y,o}$ are desired minimum force. The essential idea of this perturbation/correlation based approach is, we perturb the current position of the center of gravity of the male connector, and see the force response. While doing this, we estimate the gradient of the performance index with respect to the position of the center of gravity so that we continuously update this position based on this gradient value in order to reduce the performance index. The coordinates of the male and the female connector are defined with respect to the origin as in Figure 6-3. Our assumption is that the exact dimension of each connector is known, but the position of the female connector is not exactly known.

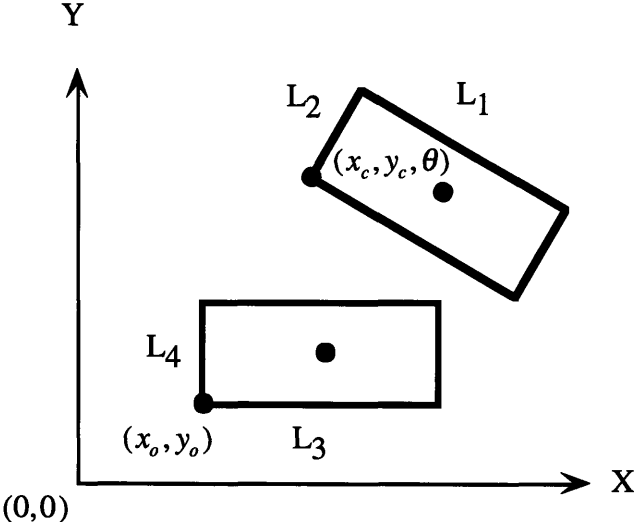


Figure 6-3. Coordinates

The exact location of the female connector, (x_o, y_o) is not known, but the two points of the male connector, (x_1, y_1) and (x_2, y_2) can be represented with respect to the center point, (x_c, y_c, θ) as shown in Figure 6-4.

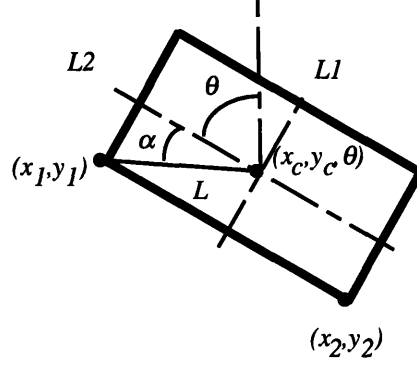


Figure 6-4. Contact Points Coordinates

$$\alpha = \tan^{-1}\left(\frac{L_2}{L_1}\right) \quad (6-4)$$

$$L = \frac{1}{2}\sqrt{L_1^2 + L_2^2} \quad (6-5)$$

$$x_1 = x_c - L\sin(\theta + \alpha) \quad (6-6)$$

$$y_1 = y_c + L\cos(\theta + \alpha) \quad (6-7)$$

$$x_2 = x_c + L\sin(\theta - \alpha) \quad (6-8)$$

$$y_2 = y_c - L\cos(\theta - \alpha) \quad (6-9)$$

Due to the stiffness of the connector, the depth of the penetration of the male connector to the female connector is,

$$\Delta x_2 = x_o + L_3 - x_2 \quad (6-10)$$

$$\Delta x_2 = x_o + L_3 - x_c - L\sin(\theta - \alpha) \quad (6-11)$$

$$\Delta y_1 = y_o + L_4 - y_1 \quad (6-12)$$

$$\Delta y_1 = y_o + L_4 - y_c - L\cos(\theta + \alpha) \quad (6-13)$$

If we assume the wall has stiffness, K_x and K_y , which are unknown, then, the response force would be,

$$F_{y1} = K_y \Delta y_1 \quad (6-14)$$

when $\Delta y_1 > 0$

$$F_{y1} = 0 \quad (6-15)$$

when $\Delta y_1 \leq 0$

$$F_{x2} = K_x \Delta x_2 \quad (6-16)$$

when $\Delta x_2 > 0$

$$F_{x2} = 0 \quad (6-17)$$

when $\Delta x_2 \leq 0$

and the coulomb friction forces with unknown friction constant, μ_x and μ_y , are

$$F_{x1} = \mu_x F_{y1} \quad (6-18)$$

$$F_{y2} = \mu_y F_{x2} \quad (6-19)$$

Therefore, the resultant forces are,

$$F_x = \mu_x K_y \Delta y_1 + K_x \Delta x_2 \quad (6-20)$$

$$F_x = \mu_x K_y (y_o + L_4 - y_c + L \cos(\theta + \alpha)) + K_x (x_o + L_3 - x_c - L \sin(\theta - \alpha)) \quad (6-21)$$

$$F_y = K_y \Delta y_1 - \mu_y K_x \Delta x_2 \quad (6-22)$$

$$F_y = K_y (y_o + L_4 - y_c + L \cos(\theta + \alpha)) - \mu_y K_x (x_o + L_3 - x_c - L \sin(\theta - \alpha)) \quad (6-23)$$

The performance index, as in eq. (6-24), is

$$P.I. = (F_x - F_{x,o})^2 + (F_y - F_{y,o})^2 \quad (6-24)$$

what we want to minimize. From the expression, we can see this performance index is nonlinear and depends on many unknown variables.

6.4 Perturbation/Correlation based Control

The perturbations to the position of the center of the box are given orthogonally as in eq. (6-25) and eq. (6-26)

$$x_c = x_{c,o} + \varepsilon_x \sin(\omega_p t) \quad (6-25)$$

$$y_c = y_{c,o} + \varepsilon_y \cos(\omega_p t) \quad (6-26)$$

where, ε_x and ε_y are the amplitudes and ω_p is the frequency of the perturbation. The two points of the box are perturbed as in eq. (6-27) through eq. (6-30)

$$x_1 = x_{c,o} + \varepsilon_x \sin(\omega_p t) - L \sin(\theta + \alpha) \quad (6-27)$$

$$y_1 = y_{c,o} + \varepsilon_y \cos(\omega_p t) + L \cos(\theta + \alpha) \quad (6-28)$$

$$x_2 = x_{c,o} + \varepsilon_x \sin(\omega_p t) + L \sin(\theta - \alpha) \quad (6-29)$$

$$y_2 = y_{c,o} + \varepsilon_y \cos(\omega_p t) - L \cos(\theta - \alpha) \quad (6-30)$$

For one period of the perturbation, the correlation values are calculated based on eq. (6-31) and eq. (6-32)

$$\int_t^{t+\frac{2\pi}{\omega_p}} \delta x_c (PI) d\tau \quad (6-31)$$

$$\text{where, } \delta x_c = \varepsilon_x \sin(\omega_p t)$$

$$\int_t^{t+\frac{2\pi}{\omega_p}} \delta y_c (PI) d\tau \quad (6-32)$$

$$\text{where, } \delta y_c = \varepsilon_y \cos(\omega_p t)$$

so that we can estimate $\frac{\partial(PI)}{\partial x_c}$ and $\frac{\partial(PI)}{\partial y_c}$.

The center position of the box is updated based on eq. (6-33) and eq. (6-34)

$$\dot{x}_{c,o} = -\gamma_x \frac{\partial(PI)}{\partial x_c} \quad (6-33)$$

$$\dot{y}_{c,o} = -\gamma_y \frac{\partial(PI)}{\partial y_c} \quad (6-34)$$

Therefore, we can guide the box to the direction of reducing the performance index. In chapter 3, we showed how to select the parameters. Similar analysis can be applied to this case. The performance index in this task is defined in eq. (6-24) Let's define F as a performance index.

$$F = P.I. \quad (6-35)$$

The performance index F is a function of many variables.

$$F = F(x_c, y_c, \theta, x_o, y_o, \alpha, L, K_x, K_y, \mu_x, \mu_y, F_{x,o}, F_{y,o}) \quad (6-36)$$

However, for one period of perturbation, $[0, \frac{2\pi}{\omega}]$, all the variables remain constant except x_c , y_c and θ . First, F is expanded as

$$\begin{aligned} F[x_c(\tau + \Delta t), y_c(\tau + \Delta t), \theta(\tau + \Delta t)] = \\ F[x_c(\tau), y_c(\tau), \theta(\tau)] + \delta x_c(t) \left. \frac{\partial F}{\partial x_c} \right|_{\tau} + \delta y_c(t) \left. \frac{\partial F}{\partial y_c} \right|_{\tau} + \delta \theta(t) \left. \frac{\partial F}{\partial \theta} \right|_{\tau} \end{aligned} \quad (6-37)$$

Correlating F and δx_c , and taking the average for one period of perturbation, we obtain,

$$\begin{aligned} \overline{\delta x_c F} \approx \int_{\tau-2\pi/\omega}^{\tau} F|_{\tau} \delta x_c dt + \\ \int_{\tau-2\pi/\omega}^{\tau} \left. \frac{\partial F}{\partial x_c} \right|_{\tau} \delta x_c(t)^2 dt + \int_{\tau-2\pi/\omega}^{\tau} \left. \frac{\partial F}{\partial y_c} \right|_{\tau} \delta x_c(t) \delta y_c(t) dt + \int_{\tau-2\pi/\omega}^{\tau} \omega t \delta x_c(t) \left. \frac{\partial F}{\partial \theta} \right|_{\tau} dt \end{aligned} \quad (6-38)$$

with δx_c and δy_c as in eq. (6-39) and eq. (6-40)

$$\delta x_c = \varepsilon_x \sin(\omega_p t) \quad (6-39)$$

$$\delta y_c = \varepsilon_y \cos(\omega_p t) \quad (6-40)$$

then, eq. (6-38) becomes

$$\overline{\delta x_c F} = \varepsilon_x^2 \pi \left. \frac{\partial F}{\partial x_c} \right|_{\tau} - \frac{2\pi \varepsilon_x}{\omega_p^2} \omega \left. \frac{\partial F}{\partial \theta} \right|_{\tau} \quad (6-41)$$

Similarly,

$$\begin{aligned} \overline{\delta y_c F} \approx \int_{\tau-2\pi/\omega}^{\tau} F_{\tau} \delta y_c(t) dt + \\ \int_{\tau-2\pi/\omega}^{\tau} \left. \frac{\partial F}{\partial x_c} \right|_{\tau} \delta x_c(t) \delta y_c(t) dt + \int_{\tau-2\pi/\omega}^{\tau} \left. \frac{\partial F}{\partial y_c} \right|_{\tau} \delta y_c^2 dt + \int_{\tau-2\pi/\omega}^{\tau} \omega t \delta y_c(t) \left. \frac{\partial F}{\partial \theta} \right|_{\tau} dt \end{aligned} \quad (6-42)$$

$$\overline{\delta y_c F} = \varepsilon_y^2 \pi \left. \frac{\partial F}{\partial y_c} \right|_{\tau} \quad (6-43)$$

Therefore to make the offset in eq. (6-41) negligible, we need a high perturbation frequency, ω_p , and a low angular velocity, ω for the box.

6.5 Simulation

In order to verify this approach, a simulation was done with the following condition.

$(x_o, y_o) = (100, 100)$ [mm]	;	location of the female connector
$(x_c, y_c, \theta) = (225, 190, \frac{\pi}{3})$ [mm][rad]	;	initial location of the male connector
$L_1 = 200, L_2 = 100$ [mm]	;	size of the male connector
$L_3 = 200, L_4 = 100$ [mm]	;	size of the female connector
$K_x = 100, K_y = 150$ [N/mm]	;	stiffness of the female connector
$\mu_x = 0.2, \mu_y = 0.1$;	friction constant
$\omega = \frac{\pi}{9}$ [rad/sec]	;	angular velocity of the male connector
$\omega_p = 40\pi$ [rad/sec]	;	perturbation frequency
$\varepsilon_x = 5, \varepsilon_y = 5$ [mm]	;	perturbation amplitude
$\gamma_x = 0.01, \gamma_y = 0.01$;	feedback gain

The performance index and the trajectories of $x_{c,o}$ and $y_{c,o}$ are shown in Figure 6-5.

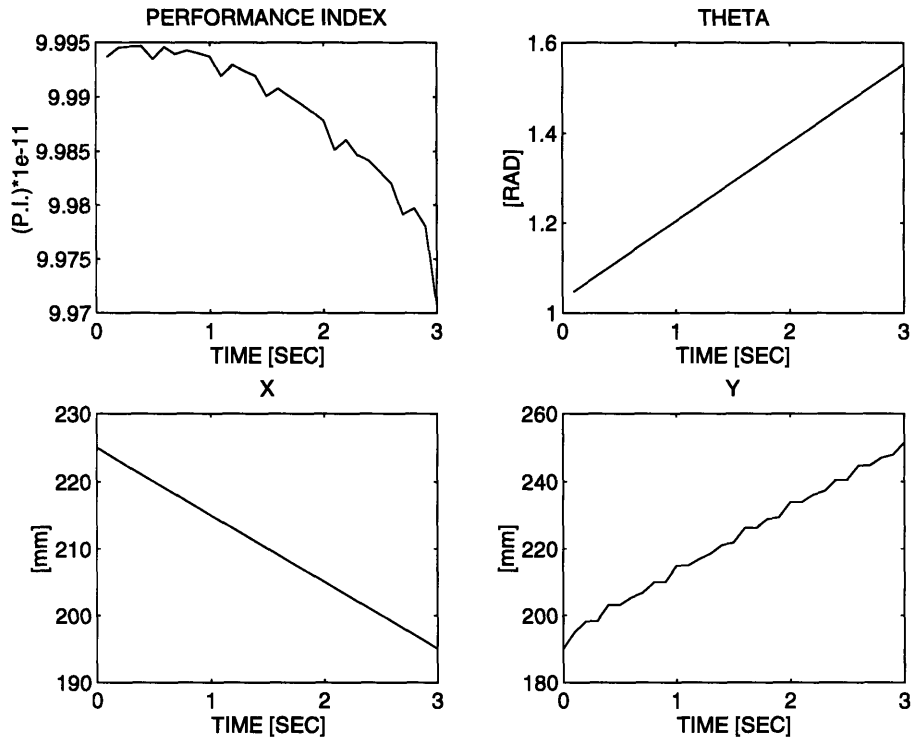


Figure 6-5. Performance Index, X, Y and θ

We can get the gradient information which guides the male connector toward the direction of reducing the performance index. The movement of the male connector is plotted in Figure 6-6.

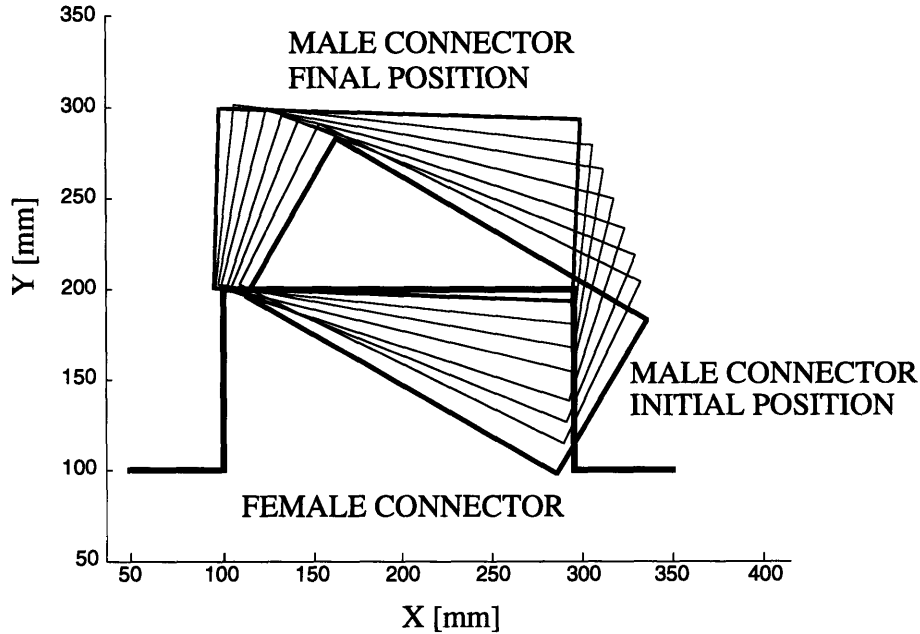


Figure 6.6 Movement of the Connector

The male connector was kept rotating at the given constant angular velocity while the center point is updated based on the control algorithm. The depth of the penetration depends on the desired minimum force response to guarantee keeping the box contacted to the wall. We can also select the resistant moment as our performance index, but we can not guarantee the box contacting both side walls with that performance index.

6.6 Comparison with Pipe Insertion Task

For another application, the perturbation/correlation based control was applied to the connector assembly task. We set up a performance index for this case and updated variables to reduce the performance index. Based on the assumption that if we could minimize the performance index, the task was done successfully, several key variables which affect the performance index were selected and controlled. For the pipe insertion

case, the pipe was perturbed to see the change of the resistant force, and for the connector assembly, the male connector was perturbed to get the change of the combined forces. Similar approach can be used to other tasks, in which minimizing a performance index leads to finish the task. In the pipe insertion case, the insertion speed was chosen as small to avoid the offset term in the estimation of the gradient, and similarly, the rotation speed in the connector assembly task. Table 6-1 summarizes the comparison between these two cases.

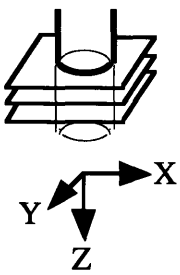
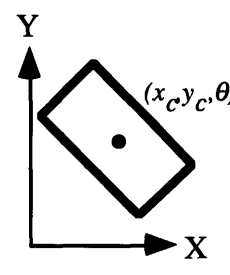
	3D Pipe Insertion	Connector Assembly
<i>Coordinate</i>		
<i>Performance Index</i>	F_z	$(F_x - F_{x,o})^2 + (F_y - F_{y,o})^2$
<i>Perturbation</i>	$\delta_x(t) = \epsilon_x \sin \omega t$ $\delta_y(t) = \epsilon_y \cos \omega t$	$\delta x_c = \epsilon_x \sin(\omega_p t)$ $\delta y_c = \epsilon_y \cos(\omega_p t)$
<i>Constant Input</i>	V_z	ω
<i>Control Law</i>	$\dot{x}_d = -\gamma_x \frac{\partial F_z}{\partial x}$ $\dot{y}_d = -\gamma_y \frac{\partial F_z}{\partial y}$	$\dot{x}_{c,o} = -\gamma_x \frac{\partial (PI)}{\partial x_c}$ $\dot{y}_{c,o} = -\gamma_y \frac{\partial (PI)}{\partial y_c}$

Table 6-1. Comparison Chart

7.1 Contributions

In this thesis, a new approach for overcoming the difficulties in the force-guided assembly for real manufacturing applications is presented. First, a performance index which clearly represents a assembly task is chosen. We set up a goal to minimize this performance index in order to accomplish the task. Then, we developed a way to guide the robot to minimize this performance index. Instead of simply receiving force information from the assembly process, we give perturbation to the robot end effector and measure the reaction forces to the given perturbation. By taking the correlation between this perturbation and the performance index, the reliable information for guiding the endeffector is extracted and used for control. This small amplitude perturbation has been used for the purpose of estimating the gradient of a performance index as well as for friction suppression.

We generalized this perturbation/correlation based control for a robot system, and then applied to the pipe insertion task which is difficult using the convention force guided control. Based on analytic model of this controller, Popov stability criterion is applied to cope with the unknown nonlinearity in the environment. Several critical assumptions are verified based on the experimental data, and the guide line to select parameters involved in this method is presented. Both simulation and experiment, the feasibility and usefulness of this approach are demonstrated. A vibratory end-effector using piezo electric actuator was designed and implemented. The same control algorithm is applied to the box palletizing task successfully.

7.1 Further Work

Some issues are still remained for further work. Even though we could get stability condition using Popov criterion, this approach is valid only for some specific nonlinearity, which belongs to a sector, and also for single input, single output case. More study on the stability for other nonlinearities should be done. To apply this method for the force-guided robotic assembly, we need to set up a performance index. This should be the one which clearly represents the assembly task. The explicit condition for the validity of a performance index for the assembly task should be derived. We have implemented vibratory end effector in order to generate high frequency perturbation for the pipe insertion task, but another methods useful for other tasks would be necessary.

Reference

- [Asada and Li, 1992] H. Asada and S.-H. Li, "Automated Robotic Assembly Using a Vibratory Work Table : Optimal Tuning of Vibrators Based on the Taguchi Method", Proc. of the Japan-USA Symposium on Flexible Automation, Vol.2, 1992
- [Cook, 1986] P. Cook, "Nonlinear Dynamical Systems", Prentice-Hall, 1986
- [Eppinger and Seering, 1986] S. Eppinger and W. Seering, "On Dynamic Models of Robot Force Control", IEEE Int. Conf. on Robotics and Automation, pp.29-34, 1986
- [Erdmann, 1986] M. Erdmann, "Using Backprojections for fine Motion Planning with the Uncertainty", Int. J. of Robotics Research, vol.5, no.1, pp.19-45, 1986
- [Hanafusa and Asada, 1977] H. Hanafusa, and H. Asada, "A Robotic Hand with Elastic Fingers and Its Application to Assembly Processes", Proc. of IFAC Symp. on Industrial Robots, pp.361-377, 1977
- [Lee and Asada, 1994] S. Lee and H. Asada, "Assembly of Parts with Irregular Surfaces Using Active Force Sensing", Proc. of the IEEE Int. Conf. on Robotics and Automation, 1994
- [Lee and Asada-1, 1995] S. Lee and H. Asada, "Direct Adaptive Control of Force-Guided Assembly Using Tuned Dither", The 1995 American Control Conference, 1995
- [Lee and Asada-2, 1995] S. Lee and H. Asada, "Use of Dither for Force-Guided Robot Control", ASME International Mechanical Engineering Congress and Exposition, 1995
- [McCarragher, Asada, 1993] B.J. McCarragher and H. Asada, "Qualitative Template Matching Using Dynamic Process Models for State Transition Recognition of Robotic Assembly", ASME Journal of Dynamic Systems , Measurement, and Control, 1993
- [Narendra and Annaswamy, 1989] K.S.Narendra and A.M.Annaswamy, "Stable Adaptive Systems", Prentice-Hall, 1989

- [Peshkin, 1992] M.A. Peshikin, "Admittance Matrix Design for Force-Guided Assembly", IEEE Transactions on Robotics and Automation, Vol. 8. No.2, 1992
- [Salisbury, 1980] J.K. Salisbury, "Active Stiffness Control of a Manipulator in Cartesian Coordinates", Proc. of the 19th IEEE Conf. on Decision and Control, pp.95-100, 1980
- [Sanders, Verhulst, 1985] J.A. Sanders, F. Verhulst, "Averaging Methods in Nonlinear Dynamical Systems", Springer-Verlag, 1985
- [Whitney, 1977] D.E. Whitney, "Force Feedback Control of Manipulator Fine Motions", ASME J. of DSMC, vol.99, no.2, pp91-97, 1977
- [Whitney, 1982] D.E. Whitney, "Quasi-Static Assembly of Compliantly Supported Rigid Parts", Journal of Dynamic Systems, Measurement and Control, pp.65-77, 1982